

## Journal Pre-proofs

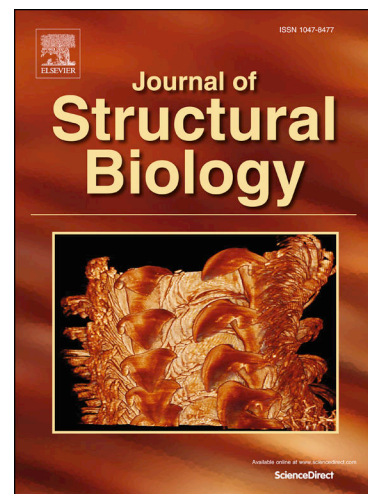
The role of the half-turn in determining structures of Alzheimer's A $\beta$ , its mutants

Steven Hayward, Akio Kitao

PII: S1047-8477(21)00097-6  
DOI: <https://doi.org/10.1016/j.jsb.2021.107792>  
Reference: YJSBI 107792

To appear in: *Journal of Structural Biology*

Received Date: 18 June 2021  
Revised Date: 10 August 2021  
Accepted Date: 29 August 2021



Please cite this article as: Hayward, S., Kitao, A., The role of the half-turn in determining structures of Alzheimer's A $\beta$ , its mutants, *Journal of Structural Biology* (2021), doi: <https://doi.org/10.1016/j.jsb.2021.107792>

This is a PDF file of an article that has undergone enhancements after acceptance, such as the addition of a cover page and metadata, and formatting for readability, but it is not yet the definitive version of record. This version will undergo additional copyediting, typesetting and review before it is published in its final form, but we are providing this version to give early visibility of the article. Please note that, during the production process, errors may be discovered which could affect the content, and all legal disclaimers that apply to the journal pertain.

© 2021 Elsevier Inc. All rights reserved.

# The role of the half-turn in determining structures of Alzheimer's A $\beta$ and its mutants

Steven Hayward<sup>a\*</sup> and Akio Kitao<sup>b\*</sup>

<sup>a</sup>Laboratory for Computational Biology, School of Computing Sciences, University of  
East Anglia, Norwich, U.K.

<sup>b</sup>School of Life Science and Technology, Tokyo Institute of Technology, 2-12-1  
Ookayama, M6-13, Meguro, Tokyo 152-8550, Japan

\*Correspondence to:

Dr Steven Hayward, Laboratory for Computational Biology, School of Computing  
Sciences, University of East Anglia, Norwich, U.K. [steven.hayward@uea.ac.uk](mailto:steven.hayward@uea.ac.uk)

Professor Akio Kitao, School of Life Science and Technology, Tokyo Institute of  
Technology, 2-12-1 Ookayama, M6-13, Meguro, Tokyo 152-8550, Japan.

[akitao@bio.titech.ac.jp](mailto:akitao@bio.titech.ac.jp)

## ABSTRACT

Half-turns are shown to be the main determinants of many experimental Alzheimer's A $\beta$  fibril structures. Fibril structures contain three half-turn types,  $\beta\alpha_R\beta$ ,  $\beta\alpha_L\beta$  and  $\beta\epsilon\beta$  which each result in a  $\sim 90^\circ$  bend in a  $\beta$ -strand. It is shown that only these half-turns enable cross- $\beta$  stacking and thus the right-angle fold seen in fibrils is an intrinsic feature of cross- $\beta$ . Encoding a strand as a conformational sequence in  $\beta$ ,  $\alpha_R$ ,  $\alpha_L$  and  $\epsilon(\beta_L)$ , pairwise combination rules for consecutive half-turns are used to decode this sequence to give the backbone path. This reveals how structures would be dramatically affected by a deletion. Using a wild-type A $\beta$ (42) fibril structure and the pairwise combination rules, the Osaka deletion is predicted to result in exposure of surfaces that are mutually shielding from the solvent. Molecular dynamics simulations on an 11-mer  $\beta$ -sheet of Alzheimer's A $\beta$ (40) of the Dutch (E22Q), Iowa (D23N), Arctic (E22G), and Osaka (E22 $\Delta$ ) mutants, show the crucial role glycine plays in the positioning of  $\beta\alpha_R\beta$  half-turns. Their "in-phase" positions along the sequence in the wild-type, Dutch mutant and Iowa mutant means that the half-folds all fold to the same side creating the same closed structure. Their out-of-phase positions in Arctic and Osaka mutants creates a flatter structure in the former and an S-shape structure in the latter which, as predicted, exposes surfaces on the inside in the closed wild-type to the outside. This is consistent with the gain of interaction model and indicates how domain swapping might explain the Osaka mutant's unique properties.

**Keywords:** Amyloid; domain swapping; familial mutants; MD simulation

## INTRODUCTION

Amyloid arises from the aggregation of misfolded proteins and is implicated in a number of human diseases including Alzheimer's Disease, Parkinson's Disease, type II diabetes and Huntington's Disease (Chiti and Dobson, 2017; Eisenberg and Jucker, 2012). The misfolded proteins assemble to form a fibrillar structure that is composed largely of  $\beta$ -sheet. Prior to formation of the insoluble fibre, misfolded proteins assemble to form a smaller, soluble structure, the amyloid intermediate which is known to be toxic (Kayed et al., 2003). For Alzheimer's amyloid- $\beta$  peptide ( $A\beta$ ) there is a heterogeneous "soup of oligomers" of varying sizes (Benilova et al., 2012) and it is thought that toxicity is the consequence of some of these oligomers embedding in the cellular membrane, compromising membrane integrity. One possibility, is that toxicity is due to oligomers forming pores in the membrane that enable ions to pass freely, disrupting ionic balance (Arispe et al., 1993). The ability of  $A\beta$  oligomers to embed in membranes suggests that they could form  $\beta$ -barrels and some experimental evidence that  $A\beta(42)$  adopts a  $\beta$ -barrel structure within a membrane-like environment has been presented (Serra-Batiste et al., 2016). Jang et al. (Jang et al., 2010) created models of membrane embedded  $\beta$ -barrels based on the experimental structure of  $A\beta$  in the fibril state and recent molecular dynamics (MD) simulations revealed the formation of  $\beta$ -barrel motifs in an  $A\beta(42)$  trimer derived from a solution structure of the monomer (Nguyen et al., 2020).

For the fibrils themselves, early X-ray fibre diffraction experiments on amyloid fibrils indicated a cross- $\beta$  structure (Sunde and Blake, 1998), that is the  $\beta$ -strands run perpendicular to the fibril axis, and numerous atomic structures of fibrils of  $A\beta(40)$  and  $A\beta(42)$  solved mainly using solid-state NMR (Colvin et al., 2016; Gremer et al., 2017; Luhrs et al., 2005; Schutz et al., 2015; Sgourakis et al., 2015) have their  $\beta$ -

strands in this arrangement. The existence of cross- $\beta$  has effectively become a defining characteristic of amyloid fibrils (Ke et al., 2020) and although there is a great deal of polymorphism within A $\beta$  fibrils (Fandrich et al., 2009; Meinhardt et al., 2009), there seems to be only one experiment where a violation of this apparent rule was found. X-ray fibre diffraction experiments performed by Fraser et al. (Fraser et al., 1992) on human A $\beta$ (40) fibrils found that the strands were tilted by 36° to the usual perpendicular arrangement of cross- $\beta$ . Further work by Malinchik et al. (Malinchik et al., 1998) suggested a model whereby a fibril comprises three to five tubular protofilaments, each of ~30 Å diameter with tilted arrays of  $\beta$ -chains. A weak meridional reflection at 57 Å suggested to Fraser et al. (Fraser et al., 1992) that there might be a 12-strand axial repeat present. Hayward and Milner-White (Hayward and Milner-White, 2017) used an extension of the theory of the shear number in  $\beta$ -barrels for application to homomeric helical  $\beta$  structures, to present a model of the protofilament subunit which comprises a parallel  $\beta$ -sheet formed from in-register strands curled up such that the outer strands join with  $\beta$ -sheet hydrogen bonding, but with a register shift. This “ $\beta$ -strip helix” has qualities of both  $\beta$ -helix and  $\beta$ -barrel structures. The estimated diameter of the protofilament, and the tilt angle of the strands from Fraser et al. were used to determine the number of strands and the register shift at the join between the outer strands of a  $\beta$ -strip helix model (Hayward and Milner-White, 2017; Hayward and Kitao, 2019). The calculation gave 11 strands, one less than estimated by Fraser et al. from the axial repeat distance, and a register shift of 22 residues. The resulting structure is  $\beta$ -barrel-like with the same tilt angle and diameter as the transmembrane  $\beta$ -barrel, TolC in *Escherichia coli*, suggesting that it could be a candidate for the toxic oligomeric intermediate. This model has a further attractive feature in that the protofilament can form from these  $\beta$ -strip helices

as protofilament subunits, joining end-to-end with the same register shift at the join between subunits as at the join between the outer strands stabilising each individual  $\beta$ -strip helix subunit (Hayward and Kitao, 2019). This same principle applies to the amyloid fibril of the HET-s(218-289) prion (Wasmer et al., 2008), which employs a tandem pseudo repeat sequence with the appropriate register shift for stabilising both the join within each individual  $\beta$ -helix subunit and the join between  $\beta$ -helix subunits forming the fibril (Hayward and Milner-White, 2017).

In order to investigate the feasibility that 11 in-register chains of wild type (WT) A $\beta$ (40) form a stable  $\beta$ -strip helix, multiple MD simulations were performed starting from parallel  $\beta$ -sheets comprising 11 perfectly straight strands forming an untwisted  $\beta$ -sheet of A $\beta$ (40) chains (Hayward and Kitao, 2019). Despite some variation in starting conditions and terminal groups, all the structures folded up to form closed structures that were remarkably similar to the experimentally derived  $\beta$ -strip helix model based on the measurements of Fraser et al.. All final structures, which had a general helical form with some disorder at the outer edges and ends, had diameters in the range 28-35 Å and tilt angles in the range 35-37°, comparing very favourably to the experimental values of 30 Å and 36°, respectively. Contacts between the outer strands were distributed around the expected register shift of 22, although there was not extensive  $\beta$ -sheet hydrogen bonding between the outer strands. MD simulations were also performed on 10- and 12-strand sheets, but these did not form closed helical structures. However, the C-terminal region of the final 12-strand structure did resemble the structure of A $\beta$ (42) by Lührs et al., (Luhrs et al., 2005) determined using NMR techniques. These results suggest something unique about the 11-mer.

A criticism of this approach might be that the starting structures for the MD simulations are non-physical. Formation of an 11-mer will involve a complex process of interaction between existing smaller oligomers of various sizes and morphologies. However, accepting that the true 11-mer structure is at a reachable global free-energy minimum from a nearby conformation of higher free energy, starting with a structure that incorporates as much as we know (11 in-register strands forming predominantly  $\beta$ -sheet), without biasing it in any way (perfectly straight strands forming a flat untwisted  $\beta$ -sheet), would seem reasonable. At the very least the final structures should reveal local variations in structure that disrupt  $\beta$ -sheet hydrogen bonding and so possibly tell us how these structural variations relate to local sequence composition.

Here we study four familial mutations at, or close to, Glu22 of A $\beta$ (40) that can cause early-onset Alzheimer's disease and cerebral amyloid angiopathy (CAA). As Glu22 is central to A $\beta$ (40) and A $\beta$ (42) mutations at this site that alter the conformation locally are likely to have a global effect. Immunological assays support the hypothesis that single mutations at Glu22 of A $\beta$ (40) cause conformational change within the emerging aggregates that lead them to be more toxic (Hatami et al., 2017). The four mutations studied are Dutch (E22Q), Iowa (D23N), Arctic (E22G), and Osaka (E22 $\Delta$ , deletion mutation). The Dutch and Iowa A $\beta$ 40 mutants have been shown to have an enhanced rate of fibril formation compared to the WT (Van Nostrand et al., 2001) and both cause severe CAA. The Arctic A $\beta$ 40 mutant also has an increased rate of protofibril formation in comparison to the WT, and it has been suggested that it

produces Alzheimer's disease through an alternative pathogenic mechanism (Nilsberth et al., 2001), perhaps due to its high degree of polymorphism (Elkins et al., 2016). *In vitro* experiments have found that the Osaka A $\beta$ 40 mutant forms a large network of fibrillar bundles rather than the straight fibrils seen with the WT (Ovchinnikova et al., 2011). However, *in vivo* analyses have shown that although it oligomerises more readily than the WT, fibrils do not form at all (Shimada et al., 2011; Tomiyama and Shimada, 2020; Tomiyama et al., 2008).

In this study we continue the approach we took previously for WT A $\beta$ (40). We performed explicit-solvent MD simulations starting from flat, untwisted 11-strand  $\beta$ -sheet structures of Dutch, Iowa, Arctic, and Osaka A $\beta$ (40) mutants to determine the effect of these mutations on the resulting structures in comparison to our previous WT simulation results. The analysis of the results of these MD simulations made us aware of the importance of glycines and the impact of half-turns in determining the overall shape of the final structure. This led to an analysis of half-turns found in deposited structures of the A $\beta$  fibril. Half-turns have the conformational sequence  $\beta\alpha_R\beta$ ,  $\beta\alpha_L\beta$  or  $\beta\epsilon\beta$  and produce an approximately 90° change in direction of the strand (Efimov, 1993). In the context of  $\beta$ -solenoids, where like here,  $\beta$ -strands in parallel are interrupted by turns, these turns have been called “ $\beta$ -arcs” (Hennetin et al., 2006). Here we show that the in-register occurrence of a half-turn on each strand of a  $\beta$ -sheet creates a ~90° fold in the sheet and that this right-angle fold is an intrinsic feature of the cross- $\beta$  structure. We also show that pairwise combination rules for the three different types of half-turns determine the general path of the backbone in cross- $\beta$  fibril structures. This demonstrates how the deletion of the Osaka mutant dramatically alters its structure compared to the wild-type.

## METHODS

### MD simulations

All MD simulations were performed by AMBER16 (D.A. Case et al., 2016). Starting structures were perfectly flat  $\beta$ -sheets comprising 11 straight strands prepared using the process described previously (Hayward and Kitao, 2019), which involved use of the SCWRL4 program (Krivov et al., 2009) for placement of side chains. Charged groups,  $\text{NH}_3$  and  $\text{COO}$  were used for the N- and C-termini, respectively, for all simulations. The AMBER ff14SB force field was used for the peptides (Maier et al., 2015). All boxes were cubes in order to minimize possible artefacts caused by the reorientation of the peptides during a long MD simulation. The SPC/Eb model (Takemura and Kitao, 2012) was used for water and Joung-Cheatham parameters (Joung and Cheatham, 2008) for KCl ions which were distributed in the box to neutralise it and impose 0.14 M ionic strength on the system. After energy minimization, 5 ns of MD simulation was performed with positional restraints imposed on N,  $\text{C}^\alpha$ , and C' by gradually weakening the force constant from 1.0 to 0.01 kcal/mol $\text{\AA}^2$ . All MD simulations were performed using the GPU implementation of Pmemd module (Le Grand et al., 2013). Isothermal-isobaric conditions were achieved by a Langevin thermostat (Sindhikara et al., 2009) and a Berendsen barostat (Berendsen et al., 1984). Equations of motion were integrated with a time step of 2 fs. The long-range Coulomb energy was evaluated using the particle mesh Ewald method (Essmann et al., 1995). After restraints were released, MD simulation without restraints was conducted for 1  $\mu\text{s}$ , and the generated trajectories were used for the analysis.

## Contour plots and model structures

The basic modelling methods used here are described in Hayward and Milner-White (Hayward and Milner-White, 2008). The standard bond lengths and bond angles used are given in Table 1 of that article. Modelling involved use of rotation matrices and translation vectors enabling transformation between coordinate systems situated on different atoms. The Ramachandran contour plots in Figure 6 are based on two quantities,  $S_P$  and  $S_B$ . We vary the  $\phi$ ,  $\psi$  angles of the residue at the bend and keep the  $\phi$ ,  $\psi$  angles of all other residues at the ideal straight  $\beta$ -strand values of  $-120^\circ, 115.8^\circ$ . We denote the two strands flanking the bend,  $\beta_1$  and  $\beta_2$ , and the unit vectors along their helical axes as  $\mathbf{n}_{\beta 1}$  and  $\mathbf{n}_{\beta 2}$ , respectively.  $\mathbf{n}_{\beta 1}$  and  $\mathbf{n}_{\beta 2}$  were determined at each  $\phi$ ,  $\psi$  point on the Ramachandran plot for the residue at the bend (Hayward and Milner-White, 2008). This means we can calculate,  $\mathbf{n}_{\beta 12}$ , the unit vector perpendicular to the plane defined by the helical axes of  $\beta_1$  and  $\beta_2$  by evaluating the cross product of  $\mathbf{n}_{\beta 1}$  and  $\mathbf{n}_{\beta 2}$ . The unit vectors,  $\mathbf{n}_{pp1}$  and  $\mathbf{n}_{pp2}$ , each perpendicular to a selected peptide plane on  $\beta_1$  and  $\beta_2$  respectively, were also calculated. As a  $\beta$ -strand with the angles  $(-120^\circ, 115.8^\circ)$  forms an untwisted flat ribbon – the number of residues per turn being exactly two – if any one peptide plane on a strand is perpendicular to the plane defined by the helical axes of the two strands, then so will all peptide planes on that strand. Thus, the unit vectors,  $\pm \mathbf{n}_{pp1}$  and  $\pm \mathbf{n}_{pp2}$  represent all peptide planes on  $\beta_1$  and  $\beta_2$ , respectively.  $S_P$ , which is a function of  $\phi$ ,  $\psi$ , of the residue at the bend was evaluated as:

$$S_P = (\mathbf{n}_{pp1} \cdot \mathbf{n}_{\beta 12})^2 + (\mathbf{n}_{pp2} \cdot \mathbf{n}_{\beta 12})^2 \quad (1)$$

where the dot indicates the scalar product.  $S_p$  will only be zero if  $\mathbf{n}_{pp1}$  and  $\mathbf{n}_{pp2}$  are both perpendicular to  $\mathbf{n}_{\beta12}$  which would mean both sets of peptide planes are perpendicular to the plane defined by the two strands.

$S_B$ , which quantifies the angle between the two strands was evaluated as:

$$S_B = (\mathbf{n}_{\beta1} \cdot \mathbf{n}_{\beta2})^2 \quad (2)$$

Values of  $\phi$ ,  $\psi$  for which  $S_B = 0$  are where there is a 90° bend.

Poly-alanine structures shown in Figure 7 were produced using an in-house program. Structures shown in Figure 7(D-F) were created by docking two individual strands using the interactive docking tool, DockIT (Iakovou et al., 2020) ([www.haptimol.co.uk](http://www.haptimol.co.uk)). Images of structures presented in Figures 2, 4, 7 and 8 were produced using PyMol ([www.pymol.org](http://www.pymol.org)).

## RESULTS

### RMSD calculations on trajectories

We compare the mutant trajectories to the WT trajectory “11\_cube\_C\_charge” from our previous work (Hayward and Kitao, 2019). Figure 1 shows RMSD “colour-maps” between the WT and each mutant over their whole 1  $\mu$ s MD simulation trajectories.

These maps enable one to compare the folding process of each mutant to that of the WT. These clearly show that early in the folding process the Arctic and Osaka mutant display radically different behaviour with their structures diverging rapidly from that of the WT. This is particularly the case for the Osaka mutant. These plots

suggest that the Dutch and the Iowa mutants fold to a similar structure to the WT. However, the Dutch mutant folds more slowly, only reaching structures similar to the WT final structure after about 600 ns.

### **RMSD calculations of final structures**

Here we compare the final WT structure to the final mutant structures. Table 1 gives the RMSD between each final mutant structure and the final WT structure. Figure 2 shows the WT final structure and the final mutant structures. It is immediately clear that the Dutch and Iowa final structures are very similar to the WT final structure, but that the Arctic and Osaka final structures are dramatically different to it. The N-terminal regions (residues 1-21) of all the mutants, which form multi-strand partial  $\beta$ -barrels, have relatively low RMSD's (see Table 1) with the WT. In all structures including the WT, the C-terminal region is more disordered. Table 1 gives the RMSD's between the C-terminal region (residues 23-40) of the mutants and the WT, which are larger than for the N-terminal region primarily because this region is more disordered. For the Dutch and Iowa mutants, like the WT, their C-terminal regions fold onto the inside surface as defined by the N-terminal partial  $\beta$ -barrel to maintain a structure that can be generally described as a right-handed multi-strand helix. Thus, the structure forms a  $\beta$ -barrel-like structure overall with a somewhat more disordered C-terminal region. The Arctic and Osaka mutants have a different morphology in their C-terminal regions. In the Arctic mutant, the C-terminal region does not fold to the right (in a helical sense) but the strands fold inwards without any lateral movement, e.g. much like the fingers in a hand would. The Osaka mutant the C-terminal region folds to contact the outside surface defined by the partial  $\beta$ -barrel

formed by the N-terminal region. Figure 2(F) clearly illustrates the dramatic difference between the WT and the Osaka mutant.

### **Analysis of $\phi$ , $\psi$ angles of final structures**

In all simulations there is little change in conformation during the final 100 ns (see Fig S1). Thus, in order to compare the  $\phi$ ,  $\psi$  angles of individual residues between the different variants in the final structures, we averaged – taking periodicity of angles into account – each residue's  $\phi$  and  $\psi$  angles over the frames in the final 100 ns of the simulation, and also over chains C-I, that is not including the outer two chains on both sides, which have rather irregular conformations. Figure 3 shows that the Dutch and Iowa mutants have  $\phi$ ,  $\psi$  angles that are very close to those of the WT apart from the final four residues at the C-terminus. For the Arctic and Osaka mutants their  $\phi$ ,  $\psi$  angles are very close to those of the WT over the N-terminal region (residues 1-20) but differ appreciably at particular residues within the C-terminal region. For all it is noticeable from Figure 3 that the change in angles from the starting structures is appreciable at and around Gly9, Gly25, and Gly29, as well as Gly22 for the Arctic mutant. They all show an appreciable change in the  $\psi$  angle of the Pre-gly from that of a  $\beta$ -sheet. If we denote the Pre-gly position as  $i$  then typical  $(\phi, \psi)$  values are  $(-130^\circ, 120^\circ)_{i-1}$ ,  $(-115^\circ, -20^\circ)_i$ , and  $(-70^\circ, 140^\circ)_{i+1}$ .

### **The “half-fold” in WT, Dutch and Iowa**

The conformational sequence based on the Ramachandran plot regions can be denoted as  $\beta(i-1)\alpha_R(i)\beta(i+1)$ , as the Pre-gly( $i$ ) is in the general right-hand  $\alpha$ -helix

region,  $\alpha_R$ , and the residue at  $i-1$  and the Gly( $i+1$ ) are in the general  $\beta$  region. If we use the finer classification of  $(\phi, \psi)$  angles in the Ramachandran plot given by Efimov (Efimov, 1993), then this conformational sequence would be  $\beta\gamma\beta_P$  where  $\gamma$  denotes a subregion of the  $\alpha_R$  region centred on  $(-90^\circ, 0^\circ)$ , and  $\beta_P$  is the polyproline II region. With standard angles  $\beta\alpha_R\beta$  produces a “half-turn” (Efimov, 1993) where there is a  $\sim 90^\circ$  change in the strand direction, but the  $\beta\gamma\beta_P$  half-turn produces a  $\sim 60^\circ$  change in strand direction. This half-turn can also be regarded as a  $\beta$ -bulge, in particular the “P-bent” class of  $\beta$ -bulge, defined by Chan et al. (Chan et al., 1993) and a type of  $\beta$ -arc (Hennetin et al., 2006). As seen in Figure 4, which shows the feature in the WT structure, the bifurcated hydrogen bonds to Pre-gly( $i$ ) and Gly( $i+1$ ) are with the carbonyl group of residue  $i-1$  on the neighbouring chain. It seems for this motif a Gly( $i+1$ ) is necessary as a side chain would be oriented to clash with neighbouring chains. The in-register arrangement of chains, means the alignment of glycines across the sheet and consequently the alignment of the half-turn. In the WT, Dutch and Iowa structures this results in half-turns in the sheet at Gly9, Gly25, and Gly29. We refer to a half-turn repeated across in-register chains as a “half-fold”.

A  $\beta$ -sheet has two sides and the side chains alternate between each side as one moves along a strand from one residue to the next. A half-fold at any one of the positions  $i, i+2, \dots$ , would cause the same side of the  $\beta$ -sheet to be on the inside of each fold, whereas a half-fold at any one of the positions  $i+1, i+3, \dots$ , would cause the opposite side of the  $\beta$ -sheet to be on the inside of each fold, i.e. they fold to opposite sides of the sheet. In the WT, Dutch and Iowa structures, Gly9, Gly25, Gly29, Gly33 and Gly37, are at odd number positions (see Figure 5). This “in-phase” arrangement means half-folds at these locations would all fold the sheet to the same

side. A  $\beta$ -sheet has a natural tendency to curl up with the strands forming right-handed helices. This is due to the natural tendency for a  $\beta$ -sheet to have a right-handed twist (Chothia, 1983) and can be clearly seen in the early stages of our folding simulations. This natural tendency means the strands in  $\beta$ -barrels always form right-handed helices. It is significant that the half-folds at Gly9, Gly25 and Gly29 in the WT, Dutch and Iowa structures all aid in the formation of a closed cylindrical structure by accentuating the natural curling of the sheet. This ability to accentuate the natural twist seen in a  $\beta$ -sheet was a feature noted by Chan et al. (Chan et al., 1993) in their study of  $\beta$ -bulges.

These considerations explain the general form of the WT, Dutch and Iowa structures and suggest an explanation for the Osaka and Arctic mutants forming such different structures. As we describe below, their structures can be explained by the “out-of-phase” positioning of the half-folds at the Gly locations in these mutants.

### **Effect of half-fold in Arctic**

The Gly22 in the Arctic mutant means we have glycines at positions 9, 22, 25, 29, 33, 37 and 38. All of these are in phase apart from Gly22 and Gly38. The effect of a half-fold at Gly22 would be expected to fold the sheet to the opposite side to that formed by the N-terminal region before it is refolded back to the same side as the N-terminal region by half-folds at Gly25 and Gly29 (see Figure 5). This is generally what we observe as the sheet has two inwardly folded regions separated by an outwardly folded kink at Gly22 (see Figure 2(D)). Although the half-fold at Gly29 shows a good array of bifurcated hydrogen bonds across the sheet, there is some

disruption of this feature at Gly22 and Gly25. This is particularly the case for Gly25 where a number of neighbouring chains on one side of the sheet have a more conventional  $\beta$ -strand configuration, whereas for the opposing set of neighbouring chains, the effect of the half-fold is plain to see.

### **Effect of half-fold in Osaka**

The Osaka mutant has a deletion at Glu22. Thus far, we have used the WT numbering to label the residues in the Osaka mutant, but if we use the actual number in the sequence then we have glycines at positions 9, 24, 28, 32, 36 and 37. Although the glycines at positions 24, 28, 32 and 36 are in phase, as a group they are out of phase with Gly9. This means a half-fold at any one of these, will fold the sheet to the opposite side to the half-fold at Gly9. What is more, they will fold to the opposite side created by the natural curl of the sheet. In the Osaka mutant, half-folds form early in the folding process particularly at Gly24 and Gly28 which causes the sheet to fold to the opposite side of the sheet to the natural curl and the half-turn at Gly9 (see Figure 5). This gives it its characteristic “S-shape” as seen in Figure 2(E). Early in the folding process there is an array of bifurcated hydrogen bonds at Gly24 and Gly28 but later in the process some of the peptide planes between the Pre-gly and Gly24, and the Pre-gly and Gly28 have rotated to disrupt these hydrogen bonds. However, the overall S-shape formed in the early stages of folding remains.

### **Half-folds in previous simulations on WT A $\beta$ 40 with 10-, 11- and 12-strands**

In our previous work we did a number of MD simulations on the A $\beta$ 40 WT with 10-, 11- and 12-strands. We performed four independent simulations with 11-strands,

each with a different starting structure, box shape or terminal groups (Hayward and Kitao, 2019). We also performed simulations on sheets formed from 10- and 12-strands. Re-analysis of the results of those simulations revealed half-folds at Gly9, Gly25 and Gly29. The C-terminal half of the 12-strand final structure bore resemblance to the solid-state NMR structure of Luhrs et al. (Luhrs et al., 2005) (PDB: 2BEG) . If we had performed simulations on the same mutants but with different size oligomers, results suggest that we would see similar effects due to the fact that the phasing of the half-turns is dependent on the positions of the glycines along the in-register chains and not on the number of strands.

### **Half-folds in experimental A $\beta$ fibril structures**

We analysed the following structures of the A $\beta$  fibril deposited in the (Protein Data Bank) PDB: the WT structures of Luhrs et al. (Luhrs et al., 2005) (PDB: 2BEG), Colvin et al. (Colvin et al., 2016) (PDB:5KK3), Gremer et al. (Gremer et al., 2017) (PDB: 5OQV) and Xiao et al. (Xiao et al., 2015), the structure of the Iowa mutant of Sgourakis et al. (Sgourakis et al., 2015) (PDB: 2MPZ), and the Osaka mutant of Schutz et al. (Schutz et al., 2015) (PDB: 2MVX). All of these, apart from the 5OQV structure, which was determined mainly using cryo-electron microscopy (cryo-EM), have been solved using NMR techniques, often solid-state NMR. All are formed from parallel  $\beta$ -sheet with their chains in-register. The in-register arrangement, combined with the cross- $\beta$  configuration, means the path of the backbone of each individual chain can be approximately represented by a single backbone trace confined to the two dimensions perpendicular to the fibril axis. Although there is a great deal of polymorphism within the 2D shapes that the backbones of the deposited structures

trace, most have one thing in common: they have straight  $\beta$ -strands interspersed by turns (in the general sense of the word) that change the path of the chain by  $\sim 90^\circ$  (see backbone traces in Figure 8). By averaging the main chain dihedral angles over the chains and models in each PDB file we were able to assign most of the turns to a  $\beta_{\alpha_R}\beta$ ,  $\beta_{\alpha_L}\beta$  or  $\beta_\epsilon\beta$  half-turn, where the  $\epsilon$  conformation (also referred to in the literature as  $\beta_L$ ) is in the lower right-hand region of the Ramachandran plot (Efimov, 1993). According to Efimov (Efimov, 1993) half-turns change the strand direction by  $\sim 90^\circ$  and so the half-turns we see in the experimental fibril structures are closer to the Efimov half-turn than the  $\beta_\gamma\beta_P$  half-turn seen in the simulations.

### **Special properties of half-turns enable cross- $\beta$ stacking**

We ask the following question: Is there a relationship between the half-turn and the cross- $\beta$  arrangement of strands? In other words, is the half-turn the only type of turn that allows the cross- $\beta$  stacking of strands? For stacking via  $\beta$ -sheet hydrogen bonding to occur, the peptide planes must be perpendicular to the plane that a bent strand creates. Any other arrangement would not result in a fibril in the cross- $\beta$  configuration. The Ramachandran contour plot shown in Figure 6(A) demonstrates that only these three half-turns give  $\beta$ -strands with their peptide planes perpendicular to the plane of the bent strand. Figure 6(B) shows that these three half-turns result in an  $\sim 90^\circ$  bend. Thus, there is a relationship between the cross- $\beta$  configuration, and the right-angle turns seen in the 2D path taken by individual chains.

In order to investigate half-turns more closely we created model structures with the  $(\phi, \psi)$  angles  $(-70^\circ, -70^\circ)$ ,  $(70^\circ, 70^\circ)$  and  $(150^\circ, -150^\circ)$ , for the  $\alpha_R$ ,  $\alpha_L$  and  $\epsilon$  conformations, respectively, the locations of which are indicated in Figure 6 on the

Ramachandran contour plots. We attempted to dock two model half-turn poly-alanine strands of each type using the interactive docking tool, DockIT (Iakovou et al., 2020), which is able to show hydrogen bonds as they form. As shown in Figure 7 (D), (E) and (F) the bent strands can be brought together such that all main-chain hydrogen bond donors and acceptors are satisfied by hydrogen bonds. For the  $\beta\epsilon\beta$  half-turn strand this could only be achieved with a glycine in the  $\epsilon$  conformation, necessary anyway for this conformation (Richardson and Richardson, 1989). These features show how the special characteristics of half-turns enable chains from separate molecules to stack in the cross- $\beta$  configuration without loss of inter-strand main-chain hydrogen bonding to build protofilaments containing half-folds.

### Pairwise combination rules for half-turns

In half-turns the direction of turn can be found using the following rule: point the thumb of corresponding hand (right for  $\beta\alpha_R\beta$ ; left for  $\beta\alpha_L\beta$  and  $\beta\epsilon\beta$ ) in direction of N-H at residue  $i-1$  (first  $\beta$  residue) and the curl of fingers gives direction of turn (see Figure 7(A), (B) and (C)). The  $\beta\alpha_R\beta$  and  $\beta\alpha_L\beta$  half-turns produce a change of phase in the orientation of the peptide planes in that if the N-H bond of residue  $i$  is pointing upwards, then the N-H of the following residue at  $i+1$  will also point upwards, whereas for the  $\beta\epsilon\beta$  half-turn the peptide planes continue to alternate in orientation (see Figure 7). Note that the  $\beta\epsilon\beta$  half-turn has a less abrupt  $90^\circ$  bend than the  $\beta\alpha_R\beta$  and  $\beta\alpha_L\beta$  half-turns and the repeating dipeptide  $\dots\beta\epsilon\beta\epsilon\beta\epsilon\dots$  forms a ring structure, called the “unpleated  $\beta$ ” (Hayward et al., 2014). Table 2 summarises the effect of the three different types of half-turns.

Consideration of handedness of half-turns and the change in phase of the orientation of the peptide planes leads to a set of rules for pairs of half-turns in  $\beta$ -strands. A pair of consecutive half turns can either produce a “reversal” as shown in Figure 7(G) or a “crankshaft” as shown in Figure 7(H). In general, reversals are produced by  $\alpha_R \dots \alpha_R$  or  $\alpha_L \dots \alpha_L$  separated by an even number of  $\beta$  residues, or by  $\alpha_R \dots \alpha_L$  and  $\alpha_L \dots \alpha_R$ , separated by an odd number of  $\beta$  residues. Crankshafts are produced by  $\alpha_R \dots \alpha_R$  or  $\alpha_L \dots \alpha_L$ , separated by an odd number of  $\beta$  residues, or by  $\alpha_R \dots \alpha_L$  and  $\alpha_L \dots \alpha_R$ , separated by an even number of  $\beta$  residues. Considering all three half-turn types, there are 18 possible pairwise combinations of half-turns; Table 2 shows which produce reversals, and which produce crankshafts. Note the rules for the  $\alpha_R$  pairs do not apply to the  $\beta\gamma\beta_P$  half-turn found in the simulations due to its very different nature.

Note that if we have  $\beta\alpha_R\alpha_L\beta$  or  $\beta\alpha_L\alpha_R\beta$  or longer sequences of alternating  $\alpha_R$  and  $\alpha_L$  conformations then this is an  $\alpha$ -strand as found in  $\alpha$ -sheet (Daggett, 2006; Hayward and Milner-White, 2008; Milner-White et al., 2006; Pauling and Corey, 1951), a secondary structure implicated in the formation of the amyloid intermediate (Hayward and Milner-White, 2021; Shea et al., 2019). Like  $\beta$ -strand,  $\alpha$ -strand is straight, but unlike the  $\beta$ -strand all N-H bonds point in the same direction.

### **Half-turn sequence representation of backbone traces of experimental A $\beta$ fibril chains**

We have assigned each residue in the six experimental structures analysed to one of either a  $\beta$ ,  $\alpha_R$ ,  $\alpha_L$ , or  $\epsilon$ . Figure 8(A) shows the alignment of these conformational

sequences. As can be seen the conformational sequence can be written in a condensed form. For the Iowa mutant, 2MPZ, the sequence is “10L1R13”, which means, starting from the N-terminus, there are 10  $\beta$  residues, followed by one  $\alpha_L$  residue, followed by one  $\beta$  residue, followed by one  $\alpha_R$  residue, followed by 13  $\beta$  residues. Using this “half-turn sequence” we can use the rules in Table 2 to produce a simplified path of the backbone. For each of the six structures studied, Figure 8(B-G) shows the half-turn sequence derived model in comparison to the backbone trace. As can be seen the half-turn sequence model follows closely the actual backbone trace in most cases, although as explained in the legend to Figure 8 for two cases the half-turn sequence model produces an overlapping structure and some adjustment is needed for it to follow the true backbone trace.

### **Modelling the Osaka mutant from the WT**

A deletion will result in an odd number of intervening  $\beta$  residues becoming even, or vice-versa, which will mean a reversal becoming a crankshaft, or a crankshaft becoming a reversal (see Table 2). The effect of a deletion can be understood clearly by appreciating that it is the equivalent to the transformation required to fit a residue at  $i$  to the previous residue at  $i-1$  in a  $\beta$ -strand. This transformation is a  $\sim 180^\circ$  rotation about, and a  $-3.3 \text{ \AA}$  translation along, a screw axis co-linear with the strand pointing in the positive strand direction. This transformation produces a crankshaft from a reversal or vice-versa.

The structure 5OQV of A $\beta$ 1-42 is a full-length structure of the WT peptide determined to  $4 \text{ \AA}$  resolution with cryo-EM complemented by solid-state NMR. It has

the half-turn sequence of 9L12L1R8L2L5 and the half-turn sequence model is shown in Figure 9(A). For the Osaka mutant structure, the deletion of Glu22 results in the half-turn sequence 9L11L1R8L2L5. Thus, the reversal L12L in the WT structure becomes the crankshaft L11L in the Osaka mutant. Figure 9(A) also shows the half-turn sequence model of the predicted Osaka mutant whereby the C-terminal side is rotated and translated by the deletion to produce a crankshaft rather than a reversal. Although this structure does not resemble the Osaka mutant structure of Schutz et al. (Schutz et al., 2015) (PDB: 2MVX) (see Figure 8(D)), the effect of the mutation is similar to what we have seen in the simulations in that the closed curled-up WT structure now has surfaces that were on the inside of a closed structure exposed to the outside. In this case two hydrophobic surfaces that mutually shield each other from the solvent in the WT are exposed in the predicted Osaka mutant. Figure 9(B) illustrates protofilaments that join together to shield the two surfaces, each now from a different protofilament. This process of association may offer a plausible explanation for the different oligomerisation behaviour of the Osaka mutant compared to the WT.

## DISCUSSION

The motivation for performing simulations on A $\beta$ (40) mutants was to compare results to the simulations performed previously on WT A $\beta$ (40) (Hayward and Kitao, 2019).

The WT 11-mer formed a structure with dimensions almost exactly matching those of the 11-strand  $\beta$ -strip helix predicted from X-ray fibre diffraction experiments by Fraser et al. (Fraser et al., 1992). A  $\beta$ -strip helix has aspects of both a  $\beta$ -helix and a  $\beta$ -barrel, and its similarity to the latter indicates that it could embed in membranes as

suggested for the toxic oligomeric intermediate. Its similarity to the former could also explain how a protofilament could form from  $\beta$ -strip helices joining end-to-end in the same way as in the HET-s(218-289) prion, although such a structure would be an exceedingly rare fibril polymorph in not having the cross- $\beta$  configuration. Such a protofilament would have a  $\beta$ -strip helix repeat distance of  $\sim 60$  Å (Hayward and Milner-White, 2017; Hayward and Kitao, 2019) which is close to the 57 Å (Fraser et al., 1992) axial repeat distance suggested by a weak meridional reflection, a quantity not used for the modelling of the 11-strand  $\beta$ -strip helix. Fraser et al. suggested this might be due to a 12-strand repeating unit, but this would not be consistent with the off-meridional 4.7 Å reflection, suggesting the strands were tilted by  $36^\circ$  to the perpendicular. There is evidence that a 12-mer soluble oligomeric species of A $\beta$ (42) causes memory loss in a transgenic mouse model (Lesne et al., 2006). This species of oligomer was referred to as A $\beta^*$ 56, 56 kDa being the molecular weight of the 12-mer. However, the results of that study would also seem not to be able to definitively exclude the possibility of an 11-mer. This begs the question – why is evidence for the 11-strand  $\beta$ -strip helix not seen by others as a fibril component? Fraser et al. found their WT fibril was not stable in aqueous solution compared to other fibrils that presented the standard cross- $\beta$  4.7 Å reflection on the meridian, requiring special treatment to stabilise it. This makes sense as the cross- $\beta$  configuration maximises inter-subunit hydrogen bonding with even those residues at the folds participating in main-chain hydrogen bonding, whereas the protofilament built from 11-strand  $\beta$ -strip helices has an inherent weakness at the join between the  $\beta$ -strip helices, where maximally only 18 ( $18=40-22$ , where 22 is the register shift) of the 40 residues participate in  $\beta$ -sheet hydrogen bonding. This may suggest that only oligomers that are in the cross- $\beta$  configuration emerge from the “oligomeric soup” (Benilova et al.,

2012) as fibrils, but those that are non-cross- $\beta$  are too weak to under most environmental conditions. However, they may be good candidates for the toxic oligomeric intermediate, especially if they have characteristics of transmembrane  $\beta$ -barrels.

Despite the considerable differences between the 11-strand  $\beta$ -strip helix model and the deposited cross- $\beta$  fibril structures, our simulations have revealed features that they have in common, namely half-turns. Previously we noted the bends in the  $\beta$ -strands at glycines in the 11-mer structure (Hayward and Kitao, 2019), but this was not explored further. These disruptions were also seen in 10-mer and 12-mer structures from our previous simulations (Hayward and Kitao, 2019). Here further analysis has shown them to be half-turns of the form  $\beta_{\alpha_R}\beta$ , more specifically  $\beta_{\gamma}\beta_P$ , with the glycine at the  $\beta_P$  position. The  $\beta_{\gamma}\beta_P$  half-turn is somewhat different to the  $\beta_{\alpha_R}\beta$  half-turn seen in the experimental A $\beta$  fibril structures, in that the latter produces an approximately 90° change in direction of the strand, whereas the former gives an approximately 60° change in strand direction. The in-register arrangement of the chains means the half-turn is generally repeated across the chains to form what we have called a “half-fold”. A recurring glycine is found at the second  $\beta$  position in a half-fold, that runs along one corner of the triangular  $\beta$ -helix in the fibril-like tail spike of T4 phage (van Raaij et al., 2001), indicating that our finding is not an artefact of simulation.

As we have demonstrated, the half-turns in the deposited cross- $\beta$  structures are of three types:  $\beta_{\alpha_R}\beta$ ,  $\beta_{\alpha_L}\beta$  and  $\beta_{\epsilon}\beta$ . Using the nomenclature of  $\beta$ -arcs (Hennetin et al., 2006), these turns would be denoted as *ba*, *bl* and *beb*, respectively. These  $\beta$ -arcs

are the shortest of the  $\beta$ -arcs types. Significantly, their hydrogen bond donor and acceptor groups can also participate in inter-strand hydrogen bonding adding more stability to the fibril than would be the case with longer  $\beta$ -arcs. That half-turns produce a  $\sim 90^\circ$  fold in a  $\beta$ -sheet means that this right-angle fold commonly seen in  $A\beta$  fibril structures is an essential feature of the cross- $\beta$  configuration.

The  $\beta\alpha_L\beta$  (more specifically,  $\beta_P\alpha_L\beta_P$ ) turn has been found to occur at the corners in left-handed  $\beta$ -helices with the equilateral prism fold (Iengar et al., 2006), but analysis of sequence features found glycine to occur at the first  $\beta_P$  position rather than the second. Certainly, glycine is required for the  $\epsilon$  conformation in the  $\beta\epsilon\beta$  half-turn. Figure 8(A) suggests that there is a connection between glycine location and the occurrence of at least some of the half-folds in the deposited fibril structures. It is intriguing to realise that the glycines are positioned to be in-phase for the  $\beta\alpha_R\beta$  fold in the WT and that this in-phase relationship means that for the WT, as well as the Dutch and Iowa mutants, the half folds all fold to the same side creating a closed, curled-up structure. Thus our conclusion would be that for the Dutch and Iowa mutants there is little impact on the fundamental structural component of  $A\beta(40)$  oligomers and the effect of these mutations may lay elsewhere, perhaps by affecting aggregation rate (Chiti et al., 2003).

For the Arctic mutant the presence of Gly22 means there is an out-of-phase glycine causing it to fold outwardly until it is refolded back inwardly by Gly25 (see Figure 5). This produces a kink in the structure which due to its central location, results in a structure that is generally flatter than the WT structure. This makes the structure

more exposed to the solvent compared to the WT, possibly explaining the enhanced rate of protofibril formation seen for the Arctic mutant (Nilsberth et al., 2001) through a process that shields exposed hydrophobic residues through subunit association. Changes of this type that lead to protofilament formation have been called the “gain of interaction” (Elam et al., 2003; Nelson and Eisenberg, 2006).

For the Osaka mutant the effect of the deletion of Glu22 is to put the Gly25 and Gly37 out of phase with Gly9 and to cause the sheet of the C-terminal side to fold to the opposite side to the N-terminal side giving it an “S” shape (see Figure 5). This will put the side that is originally on the inside of the closed WT structure on the outside, and vice-versa. This is another example of the gain of interaction model.

Due to their cross- $\beta$  structure, the backbone traces of the deposited structures of A $\beta$  are largely restricted to 2D. In many cases the structures comprise  $\beta$ -strands interspersed by half-turns of which there are three types:  $\beta\alpha_R\beta$ ,  $\beta\alpha_L\beta$  and  $\beta\varepsilon\beta$ . We have shown, the main-chain conformational sequence can be decoded using pairwise combination rules for consecutive half-turns to give the trace of the backbone. As seen from Table 2, the effect of a single deletion in a  $\beta$ -strand between two half-turns would, all else remaining the same, cause a reversal to become a crankshaft or vice-versa. This will have a dramatic consequence if, in the case of a reversal, the two inside surfaces are shielding each other from the solvent. We used the full N- to C-terminal structure of the WT fibril of A $\beta$ (42) solved to a relatively high 4 Å resolution using cryo-EM (Gremer et al., 2017) to model the effect of the Osaka mutation. This structure has interdigitating side chains within a single protofilament

producing a so-called “steric zipper” arrangement (Nelson and Eisenberg, 2006). Based on the pairwise combination rules, the deletion of Glu22 turns a reversal in the WT into a crankshaft in the Osaka mutant resulting in exposure of a dry surface in the WT to the solvent. Although the final structure from our simulations on the WT does not resemble the WT fibril of A $\beta$ (42), the predicted effect of the deletion of Glu22 on the structure is in its nature the same as seen from the simulations in that surfaces that are interior become exterior and the gain of interaction model would seem to apply. As seen in Figure 9(B) two mutually shielding surfaces within a single WT subunit become exposed in the Osaka mutant allowing shielding to occur through protofilament association in a domain swapping process (Nelson and Eisenberg, 2006). This could explain the observation that the Osaka mutant forms a large network of fibrillar bundles *in vitro* (Ovchinnikova et al., 2011) rather than straight fibrils of the WT.

## CONCLUSIONS

Analysis of simulation results on A $\beta$  oligomers and experimental structures of A $\beta$  fibrils has revealed the role played by half-turns in determining structure. It has been shown that only those half-turns, which create a  $\sim 90^\circ$  bend in a strand enable the stacking of strands in the cross- $\beta$  configuration. Thus, the right-angle fold seen in many fibril structures is an intrinsic feature of the cross- $\beta$  configuration. At the fold all inter-strand hydrogen bond donors and acceptors are satisfied, suggesting a highly stable conformation. The pairwise combination rules for half-turns allow one to determine the general path of the backbone and suggest relatively simple rules could be applied for modelling A $\beta$  fibrils. For example, a relatively short distance between

two neighbouring half-folds that produce a reversal will enable side chains to interlock in a steric zipper arrangement as seen in a number of fibril structures. If half-turns occur at specific residues such as glycines, as strongly suggested by our simulations and indicated by the experimental results, then the 2D path will be largely determined by the position of glycines in the sequence. In the WT, Dutch and Iowa mutants all glycines, apart from the one closest to the C-terminal, are in-phase, which means the half-turns all fold to the same side creating a closed conformation. The out-of-phase positions of glycines in the Arctic and Osaka mutants explains their radically different final structures. Although there is obviously a large amount of variation in the 2D path seen in the deposited structures, these insights could provide a starting point for further analysis. Indeed, this insight has already provided us with a possible explanation of the Osaka mutant's tendency to form of a network of fibrillar bundles *in-vitro* by protofilament association via a domain swapping process.

## ACKNOWLEDGEMENTS

The authors thank support from Tokyo Institute of Technology "Research Abroad and Invitational for International Collaboration" programme, 2018. This research was partly supported by MEXT/JSPS KAKENHI (JP19H03191 and JP20H05439) and MEXT "Program for Promoting Researches on the Supercomputer Fugaku" (MD driven Precision Medicine) to A.K. The MD simulations were partly performed using the supercomputers at the RCCS, The National Institute of Natural Science, and ISSP, The University of Tokyo.

## SUPPLEMENTAL INFORMATION

Figure S1 showing RMSD trajectories.

## REFERENCES

- Arispe, N., Rojas, E., Pollard, H.B., 1993. Alzheimer-disease amyloid beta-protein forms calcium channels in bilayer-membranes - blockade by tromethamine and aluminum. *Proc. Natl. Acad. Sci. U. S. A.* 90, 567-571.
- Benilova, I., Karran, E., De Strooper, B., 2012. The toxic A beta oligomer and Alzheimer's disease: an emperor in need of clothes. *Nature Neuroscience* 15, 349-357.
- Berendsen, H.J.C., Postma, J.P.M., Gunsteren, W.F.v., Nola, A.D., 1984. Molecular dynamics with coupling to an external bath. *J. Chem. Phys.* 81, 3684-3690.
- Chan, A.W.E., Hutchinson, E.G., Harris, D., Thornton, J.M., 1993. Identification, classification, and analysis of beta-bulges in proteins. *Protein Science* 2, 1574-1590.
- Chiti, F., Dobson, C.M., 2017. Protein Misfolding, Amyloid Formation, and Human Disease: A Summary of Progress Over the Last Decade, p. 27-68, in: R. D. Kornberg, (Ed.), *Annual Review of Biochemistry*, Vol 86.
- Chiti, F., Stefani, M., Taddei, N., Ramponi, G., Dobson, C.M., 2003. Rationalization of the effects of mutations on peptide and protein aggregation rates. *Nature* 424, 805-808.
- Chothia, C., 1983. Coiling of Beta-Pleated Sheets. *J.Mol.Biol.* 163, 107-117.
- Colvin, M.T., Silvers, R., Ni, Q.Z., Can, T.V., Sergeyev, I., Rosay, M., Donovan, K.J., Michael, B., Wall, J., Linse, S., Griffin, R.G., 2016. Atomic Resolution

- Structure of Monomorphic A beta(42) Amyloid Fibrils. *J.Am.Chem.Soc.* 138, 9663-9674.
- D.A. Case, R.M.B., D.S. Cerutti, T.E. Cheatham, III, T.A. Darden, R.E. Duke, T.J. Giese, H. Gohlke,, A.W. Goetz, N.H., S. Izadi, P. Janowski, J. Kaus, A. Kovalenko, T.S. Lee, S. LeGrand, P. Li, C., Lin, T.L., R. Luo, B. Madej, D. Mermelstein, K.M. Merz, G. Monard, H. Nguyen, H.T. Nguyen, I., Omelyan, A.O., D.R. Roe, A. Roitberg, C. Sagui, C.L. Simmerling, W.M. Botello-Smith, J. Swails,, R.C. Walker, J.W., R.M. Wolf, X. Wu, L. Xiao and P.A. Kollman. 2016. AMBER 2016. University of California, San Francisco.
- Daggett, V., 2006. alpha-sheet: The toxic conformer in amyloid diseases? *Accounts of Chemical Research* 39, 594-602.
- Efimov, A.V., 1993. Standard Structures in Proteins. *Progress in Biophysics & Molecular Biology* 60, 201-239.
- Eisenberg, D., Jucker, M., 2012. The Amyloid State of Proteins in Human Diseases. *Cell* 148, 1188-1203.
- Elam, J.S., Taylor, A.B., Strange, R., Antonyuk, S., Doucette, P.A., Rodriguez, J.A., Hasnain, S.S., Hayward, L.J., Valentine, J.S., Yeates, T.O., Hart, P.J., 2003. Amyloid-like filaments and water-filled nanotubes formed by SOD1 mutant proteins linked to familial ALS. *Nature Structural Biology* 10, 461-467.
- Elkins, M.R., Wang, T., Nick, M., Jo, H., Lemmin, T., Prusiner, S.B., DeGrado, W.F., Stohr, J., Hong, M., 2016. Structural Polymorphism of Alzheimer's beta-Amyloid Fibrils as Controlled by an E22 Switch: A Solid-State NMR Study. *J.Am.Chem.Soc.* 138, 9840-9852.

- Essmann, U., Perera, L., Berkowitz, M.L., Darden, T., Lee, H., Pedersen, L.G., 1995. A Smooth Particle Mesh Ewald Method. *Journal of Chemical Physics* 103, 8577-8593.
- Fandrich, M., Meinhardt, J., Grigorieff, N., 2009. Structural polymorphism of Alzheimer A beta and other amyloid fibrils. *Prion* 3, 89-93.
- Fraser, P.E., Nguyen, J.T., Inouye, H., Surewicz, W.K., Selkoe, D.J., Podlisny, M.B., Kirschner, D.A., 1992. Fibril formation by primate, rodent, and dutch-hemorrhagic analogs of alzheimer amyloid beta-protein. *Biochemistry* 31, 10716-10723.
- Gremer, L., Scholzel, D., Schenk, C., Reinartz, E., Labahn, J., Ravelli, R.B.G., Tusche, M., Lopez-Iglesias, C., Hoyer, W., Heise, H., Willbold, D., Schroder, G.F., 2017. Fibril structure of amyloid-beta(1-42) by cryo-electron microscopy. *Science* 358, 116-+.
- Hatami, A., Monjazebe, S., Milton, S., Glabe, C.G., 2017. Familial Alzheimer's Disease Mutations within the Amyloid Precursor Protein Alter the Aggregation and Conformation of the Amyloid-beta Peptide. *J.Biol.Chem.* 292, 3172-3185.
- Hayward, S., Milner-White, E.J., 2008. The geometry of alpha-sheet: Implications for its possible function as amyloid precursor in proteins. *Proteins-Structure Function and Bioinformatics* 71, 415-425.
- Hayward, S., Milner-White, E.J., 2017. Geometrical principles of homomeric  $\beta$ -barrels and  $\beta$ -helices: Application to modeling amyloid protofilaments. *Proteins* 85, 1866-1881.
- Hayward, S., Kitao, A., 2019. Multi-strand  $\beta$ -sheet of Alzheimer A $\beta$ (1-40) folds to  $\beta$ -strip helix: implication for protofilament formation. *Journal of Biomolecular Structure & Dynamics* 37, 2143-2153.

- Hayward, S., Milner-White, E.J., 2021. Determination of amino acids that favour the  $\alpha$ L region using Ramachandran propensity plots. Implications for  $\alpha$ -sheet as the possible amyloid intermediate. *Journal of Structural Biology* 213, 107738.
- Hayward, S., Leader, D.P., Al-Shubailly, F., Milner-White, E.J., 2014. Rings and ribbons in protein structures: Characterization using helical parameters and Ramachandran plots for repeating dipeptides. *Proteins-Structure Function and Bioinformatics* 82, 230-239.
- Hennetin, J., Jullian, B., Steven, A.C., Kajava, A.V., 2006. Standard conformations of beta-arches in beta-solenoid proteins. *J.Mol.Biol.* 358, 1094-1105.
- Iakovou, G., Alhazzazi, M., Hayward, S., Laycock, S., 2020. DockIT: A Tool for Interactive Molecular Docking and Molecular Complex Construction. *Bioinformatics* 36, 5698-5700.
- Iengar, P., Josh, N.V., Balaram, P., 2006. Conformational and sequence signatures in beta helix proteins. *Structure* 14, 529-542.
- Jang, H., Arce, F.T., Ramachandran, S., Capone, R., Lal, R., Nussinov, R., 2010. beta-Barrel Topology of Alzheimer's beta-Amyloid Ion Channels. *J.Mol.Biol.* 404, 917-934.
- Joung, I.S., Cheatham, T.E., 2008. Determination of alkali and halide monovalent ion parameters for use in explicitly solvated biomolecular simulations. *Journal of Physical Chemistry B* 112, 9020-9041.
- Kayed, R., Head, E., Thompson, J.L., McIntire, T.M., Milton, S.C., Cotman, C.W., Glabe, C.G., 2003. Common structure of soluble amyloid oligomers implies common mechanism of pathogenesis. *Science* 300, 486-489.
- Ke, P.C., Zhou, R.H., Serpell, L.C., Riek, R., Knowles, T.P.J., Lashuel, H.A., Gazit, E., Hamley, I.W., Davis, T.P., Fandrich, M., Otzen, D.E., Chapman, M.R.,

- Dobson, C.M., Eisenberg, D.S., Mezzenga, R., 2020. Half a century of amyloids: past, present and future. *Chemical Society Reviews* 49, 5473-5509.
- Krivov, G.G., Shapovalov, M.V., Dunbrack, R.L., 2009. Improved prediction of protein side-chain conformations with SCWRL4. *Proteins-Structure Function and Bioinformatics* 77, 778-795.
- Le Grand, S., Gotz, A.W., Walker, R.C., 2013. SPFP: Speed without compromise-A mixed precision model for GPU accelerated molecular dynamics simulations. *Comput. Phys. Commun.* 184, 374-380.
- Lee, R.A., Razaz, M., Hayward, S., 2003. The DynDom database of protein domain motions. *Bioinformatics* 19, 1290-1291.
- Lesne, S., Koh, M.T., Kotilinek, L., Kaye, R., Glabe, C.G., Yang, A., Gallagher, M., Ashe, K.H., 2006. A specific amyloid-beta protein assembly in the brain impairs memory. *Nature* 440, 352-357.
- Luhrs, T., Ritter, C., Adrian, M., Riek-Loher, D., Bohrmann, B., Doeli, H., Schubert, D., Riek, R., 2005. 3D structure of Alzheimer's amyloid-beta(1-42) fibrils. *Proc. Natl. Acad. Sci. U. S. A.* 102, 17342-17347.
- Maier, J.A., Martinez, C., Kasavajhala, K., Wickstrom, L., Hauser, K.E., Simmerling, C., 2015. ff14SB: Improving the Accuracy of Protein Side Chain and Backbone Parameters from ff99SB. *J Chem Theory Comput* 11, 3696-3713.
- Malinchik, S.B., Inouye, H., Szumowski, K.E., Kirschner, D.A., 1998. Structural analysis of Alzheimer's beta(1-40) amyloid: Protofilament assembly of tubular fibrils. *Biophysical Journal* 74, 537-545.
- Meinhardt, J., Sachse, C., Hortschansky, P., Grigorieff, N., Fandrich, M., 2009. A beta(1-40) Fibril Polymorphism Implies Diverse Interaction Patterns in Amyloid Fibrils. *J.Mol.Biol.* 386, 869-877.

- Milner-White, E.J., Watson, J.D., Qi, G., Hayward, S., 2006. Amyloid formation may involve alpha- to beta- sheet interconversion via peptide plane flipping. *Structure* 14, 1369-1376.
- Nelson, R., Eisenberg, D., 2006. Recent atomic models of amyloid fibril structure. *Current Opinion in Structural Biology* 16, 260-265.
- Nguyen, H.L., Linh, H.Q., Matteini, P., La Penna, G., Li, M.S., 2020. Emergence of Barrel Motif in Amyloid-beta Trimer: A Computational Study. *Journal of Physical Chemistry B* 124, 10617-10631.
- Nilsberth, C., Westlind-Danielsson, A., Eckman, C.B., Condrón, M.M., Axelman, K., Forsell, C., Stenh, C., Luthman, J., Teplow, D.B., Younkin, S.G., Naslund, J., Lannfelt, L., 2001. The 'Arctic' APP mutation (E693G) causes Alzheimer's disease by enhanced A beta protofibril formation. *Nature Neuroscience* 4, 887-893.
- Ovchinnikova, O.Y., Finder, V.H., Vodopivec, I., Nitsch, R.M., Glockshuber, R., 2011. The Osaka FAD Mutation E22 Delta Leads to the Formation of a Previously Unknown Type of Amyloid beta Fibrils and Modulates A beta Neurotoxicity. *J.Mol.Biol.* 408, 780-791.
- Pauling, L., Corey, R.B., 1951. The Pleated Sheet, a New Layer Configuration of Polypeptide Chains. *Proc. Natl. Acad. Sci. U. S. A.* 37, 251-256.
- Richardson, J.S., Richardson, D.C., 1989. Principles and patterns of protein conformations, p. 1-98, in: G. D. Fasman, (Ed.), *Prediction of protein structure and principles of protein conformation.* , Plenum Press, New York.
- Schutz, A.K., Vagt, T., Huber, M., Ovchinnikova, O.Y., Cadalbert, R., Wall, J., Guntert, P., Bockmann, A., Glockshuber, R., Meier, B.H., 2015. Atomic-

- Resolution Three-Dimensional Structure of Amyloid beta Fibrils Bearing the Osaka Mutation. *Angewandte Chemie-International Edition* 54, 331-335.
- Serra-Batiste, M., Ninot-Pedrosa, M., Bayoumi, M., Gairi, M., Maglia, G., Carulla, N., 2016. A beta 42 assembles into specific beta-barrel pore-forming oligomers in membrane-mimicking environments. *Proc. Natl. Acad. Sci. U. S. A.* 113, 10866-10871.
- Sgourakis, N.G., Yau, W.M., Qiang, W., 2015. Modeling an In-Register, Parallel "Iowa" A beta Fibril Structure Using Solid-State NMR Data from Labeled Samples with Rosetta. *Structure* 23, 216-227.
- Shea, D., Hsu, C.C., Bi, T.M., Paranjapye, N., Childers, M.C., Cochran, J., Tomberlin, C.P., Wang, L.B., Paris, D., Zonderman, J., Varani, G., Link, C.D., Mullan, M., Daggett, V., 2019. alpha-Sheet secondary structure in amyloid beta-peptide drives aggregation and toxicity in Alzheimer's disease. *Proc. Natl. Acad. Sci. U. S. A.* 116, 8895-8900.
- Shimada, H., Ataka, S., Tomiyama, T., Takechi, H., Mori, H., Miki, T., 2011. Clinical Course of Patients with Familial Early-Onset Alzheimer's Disease Potentially Lacking Senile Plaques Bearing the E693 Delta Mutation in Amyloid Precursor Protein. *Dementia and Geriatric Cognitive Disorders* 32, 45-54.
- Sindhikara, D.J., Kim, S., Voter, A.F., Roitberg, A.E., 2009. Bad Seeds Sprout Perilous Dynamics: Stochastic Thermostat Induced Trajectory Synchronization in Biomolecules. *Journal of Chemical Theory and Computation* 5, 1624-1631.
- Sunde, M., Blake, C.C.F., 1998. From the globular to the fibrous state: protein structure and structural conversion in amyloid formation. *Quarterly Reviews of Biophysics* 31, 1-+.

- Takemura, K., Kitao, A., 2012. Water Model Tuning for Improved Reproduction of Rotational Diffusion and NMR Spectral Density. *Journal of Physical Chemistry B* 116, 6279-6287.
- Tomiyama, T., Shimada, H., 2020. APP Osaka Mutation in Familial Alzheimer's Disease-Its Discovery, Phenotypes, and Mechanism of Recessive Inheritance. *International Journal of Molecular Sciences* 21.
- Tomiyama, T., Nagata, T., Shimada, H., Teraoka, R., Fukushima, A., Kanemitsu, H., Takuma, H., Kuwano, R., Imagawa, M., Ataka, S., Wada, Y., Yoshioka, E., Nishizaki, T., Watanabe, Y., Mori, H., 2008. A new amyloid beta variant favoring oligomerization in Alzheimer's-type dementia. *Annals of Neurology* 63, 377-387.
- Van Nostrand, W.E., Melchor, J.P., Cho, H.S., Greenberg, S.M., Rebeck, G.W., 2001. Pathogenic effects of D23N Iowa mutant amyloid beta-protein. *J.Biol.Chem.* 276, 32860-32866.
- van Raaij, M.J., Schoehn, G., Burda, M.R., Miller, S., 2001. Crystal structure of a heat and protease-stable part of the bacteriophage T4 short tail fibre. *J.Mol.Biol.* 314, 1137-1146.
- Wasmer, C., Lange, A., Van Melckebeke, H., Siemer, A.B., Riek, R., Meier, B.H., 2008. Amyloid fibrils of the HET-s(218-289) prion form a beta solenoid with a triangular hydrophobic core. *Science* 319, 1523-1526.
- Xiao, Y.L., Ma, B.Y., McElheny, D., Parthasarathy, S., Long, F., Hoshi, M., Nussinov, R., Ishii, Y., 2015. A beta(1-42) fibril structure illuminates self-recognition and replication of amyloid in Alzheimer's disease. *Nature Structural & Molecular Biology* 22, 499-U497.

Journal Pre-proofs

## TABLES

TABLE I RMSD of mutant final structures with WT final structure

RMSD of C $\alpha$  atoms after superposition on residues indicated.

Mutant	Whole protein RMSD (Å)	N-term RMSD (residues 1-21) (Å)	C-term RMSD (residues 23-40) (Å)
Dutch, E22Q	5.9	3.0	7.6
Iowa, D23N	7.2	3.5	9.6
Arctic, E22G	16.0	3.8	11.1
Osaka, E22Δ	18.7*	4.5	15.4*

\*RMSD is determined by fitting on corresponding residues.

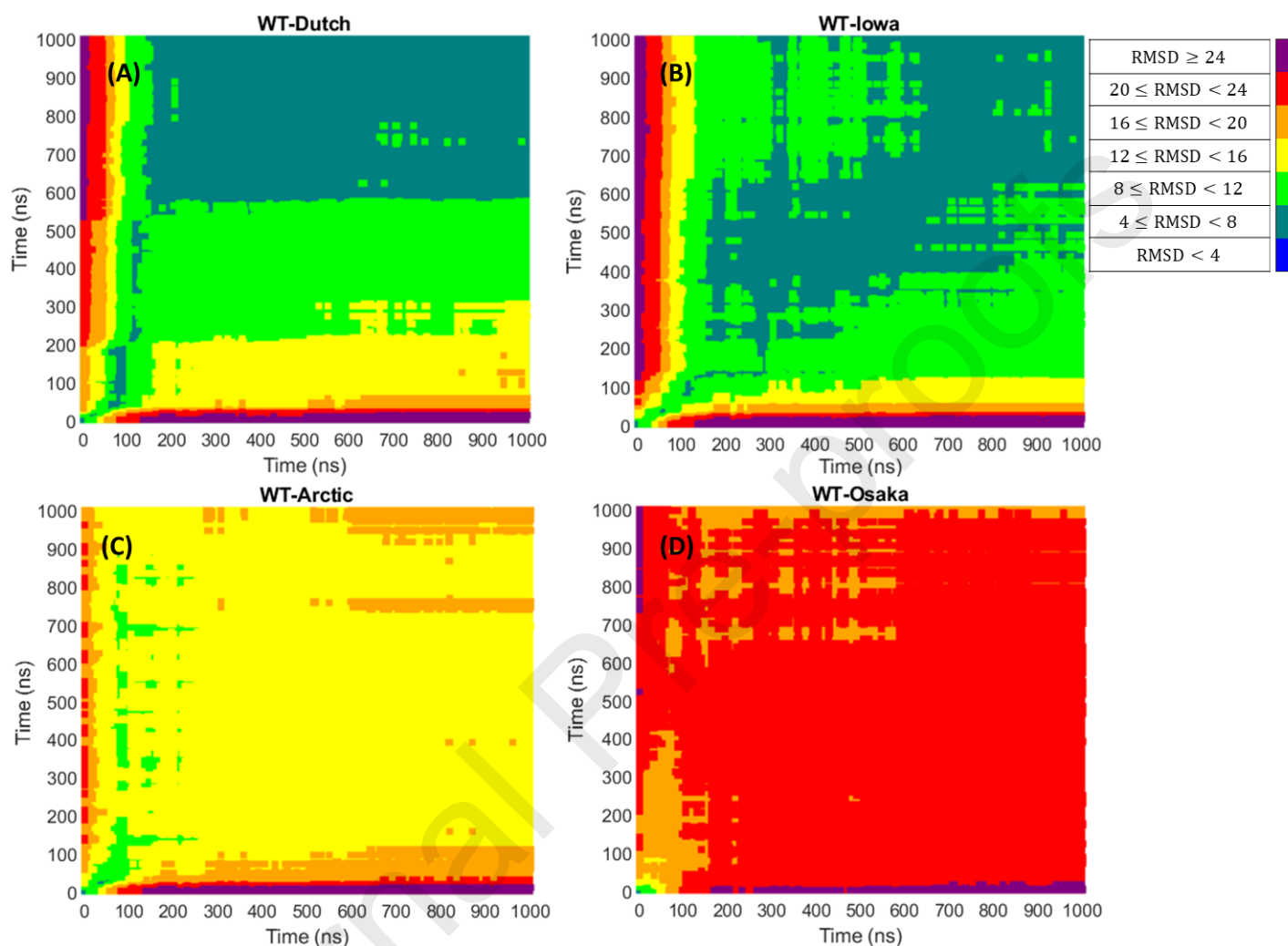
TABLE 2 Half-turn rules

Structural rules for individual half-turns		
Half-turn type	Turn direction <sup>(a)</sup>	Phase change
$\beta\alpha_R\beta$	~90° right-hand	Yes
$\beta\alpha_L\beta$	~90° left-hand	Yes
$\beta\varepsilon\beta$	~90° left-hand	No
Structural rules for pairs of half-turns		
Half-turn pair type	Even <sup>(b)</sup>	Odd <sup>(b)</sup>
$\alpha_R\dots\beta\dots\alpha_R$	Reversal	Crankshaft
$\alpha_L\dots\beta\dots\alpha_L$		
$\alpha_L\dots\beta\dots\varepsilon$		
$\varepsilon\dots\beta\dots\alpha_R$		
$\alpha_R\dots\beta\dots\alpha_L$	Crankshaft	Reversal
$\alpha_R\dots\beta\dots\varepsilon$		
$\alpha_L\dots\beta\dots\alpha_R$		
$\varepsilon\dots\beta\dots\alpha_L$		
$\varepsilon\dots\beta\dots\varepsilon$		

<sup>(a)</sup> Thumb of corresponding hand pointing in direction of N-H at residue i-1 (first  $\beta$  residue) and curl of fingers gives direction of turn (see Figure 7(A), (B) and (C)).<sup>(b)</sup> Even and odd refer to the number of intervening residues in the  $\beta$  conformation.

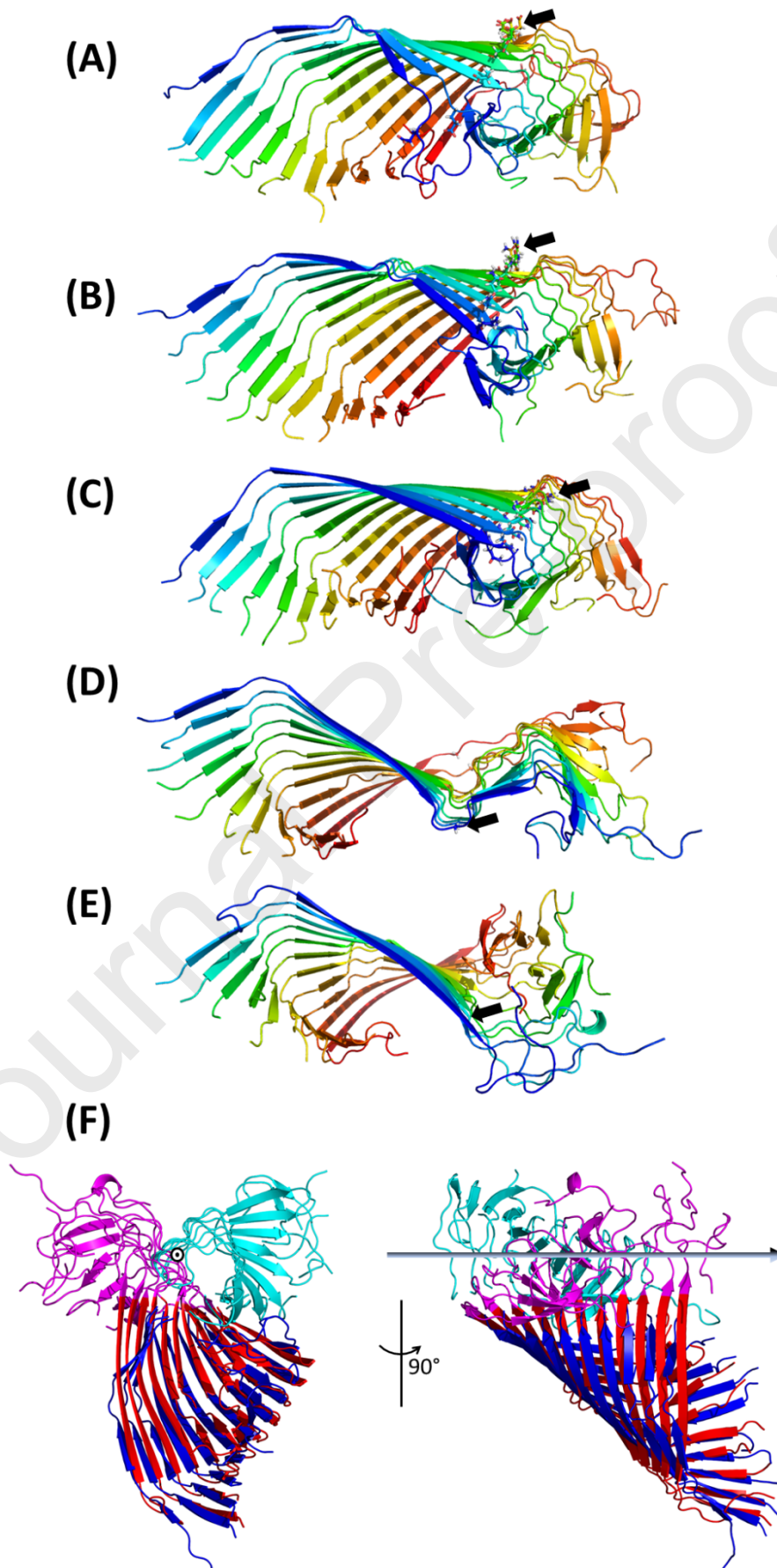
## FIGURES

Figure 1



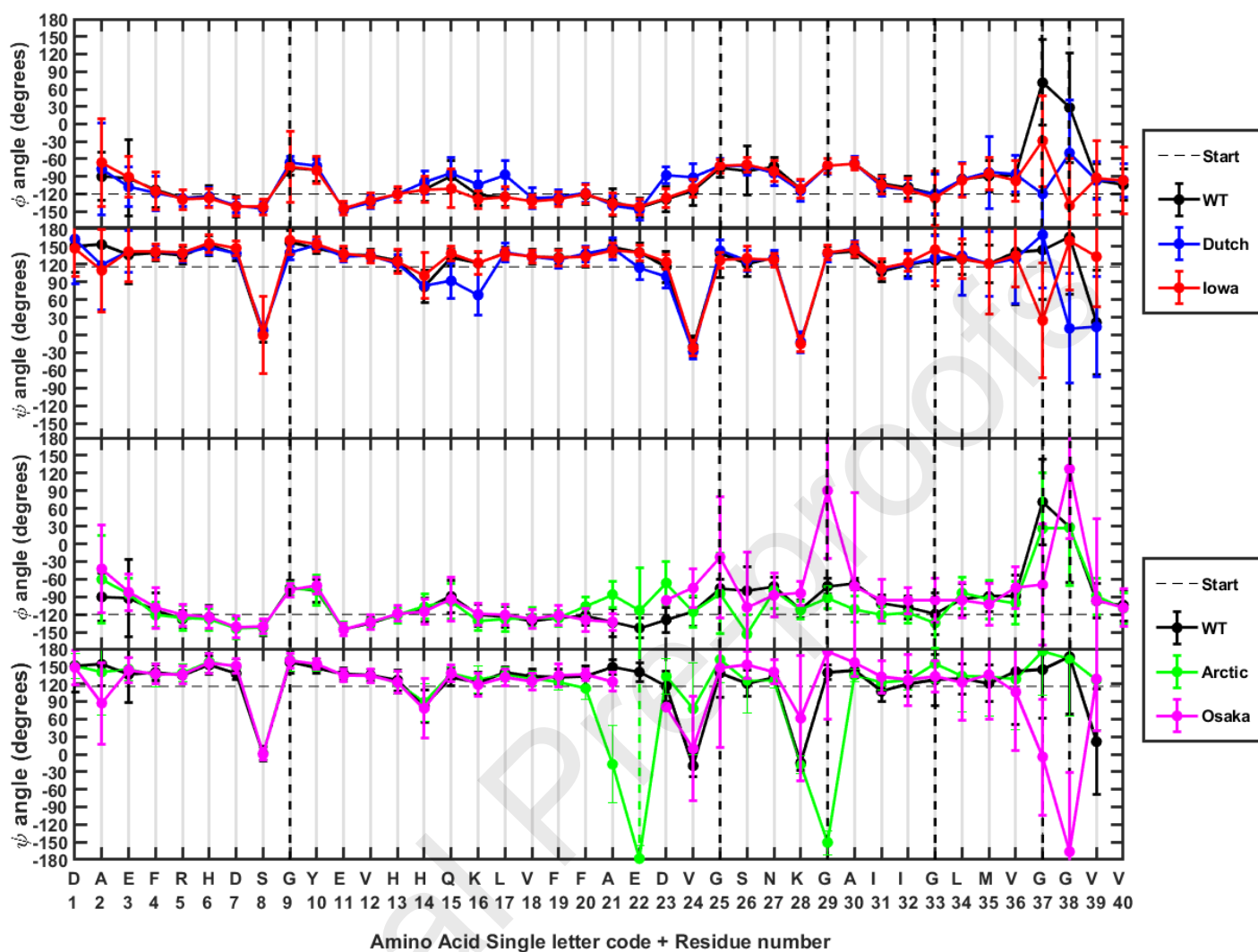
**Figure 1:** C<sup>α</sup>-atom RMSD “colour-maps” between WT and each mutant over whole trajectories. Colour coding is indicated with RMSD values given in Å. The WT time axis is along the x-axis and the mutant time axis is along the y-axis. **(A)** WT and Dutch. **(B)** WT and Iowa. **(C)** WT and Arctic. **(D)** WT and Osaka.

Figure 2



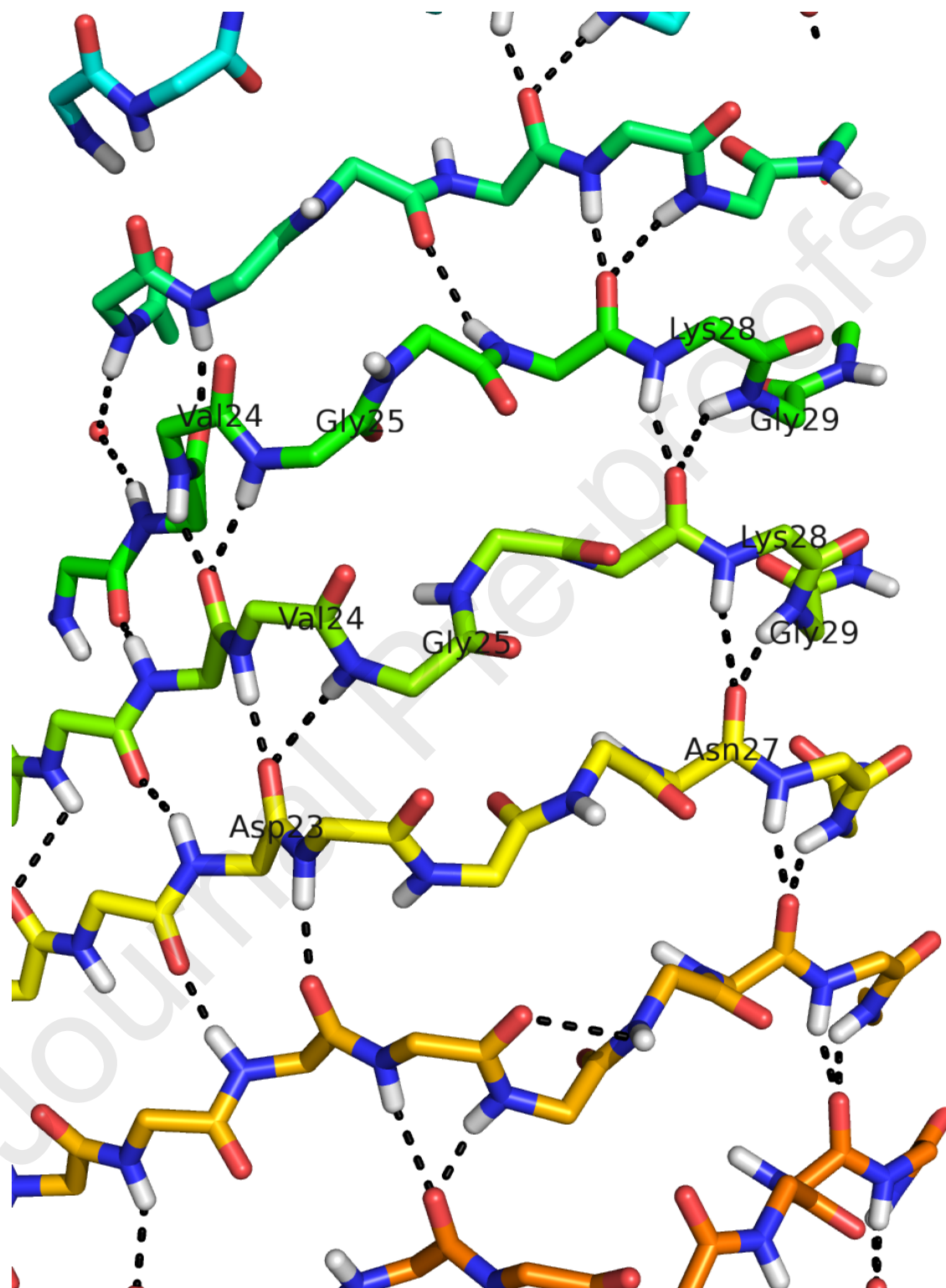
**Figure 2:** Final structures from MD simulations. **(A)** WT **(B)** Dutch (E22Q) **(C)** Iowa (D23N) **(D)** Arctic (E22G) **(E)** Osaka (E22 $\Delta$ ). The black arrows indicate locations of Glu22, Gln(22), Asn(23) and Gly22, shown in stick depiction, in (A), (B), (C) and (D), respectively, and the site of the deletion in (E). **(F)** Two views of the WT and Osaka mutant fitted on their N-terminal halves. Blue and cyan are the N-terminal and C-terminal halves of the WT, respectively; red and magenta are the N-terminal and C-terminal halves of the Osaka mutant, respectively. Glu22 in the WT is situated between the blue and cyan regions. The arrow is the screw axis for the movement of the C-terminal WT backbone to best fit with C-terminal backbone of the Osaka mutant. It rotates  $\sim 180^\circ$  about and translates  $\sim 10$  Å along the axis. Screw axis was determined using the “Domain Select” webserver at [www.cmp.uea.ac.uk/dyndom](http://www.cmp.uea.ac.uk/dyndom) (Lee et al., 2003).

Figure 3



**Figure 3:** Plots of  $\phi$  and  $\psi$  angles against residue number and amino acid single-letter code for the WT, Dutch and Iowa (top half of figure) and for the WT, Arctic and Osaka (bottom half of figure). These are mean values averaged over chains C-I and the final 100 ns. Glycine positions common to all variants are indicated by the vertical broken black lines at positions 9, 25, 29, 33, 37 and 38. The vertical broken line in green is at position 22 and only occurs in the Arctic mutant. The horizontal broken black lines are at  $\phi = -120^\circ$  and  $\psi = 115.8^\circ$  which are the values for the starting structures. The error bars show one standard deviation from the mean.

Figure 4



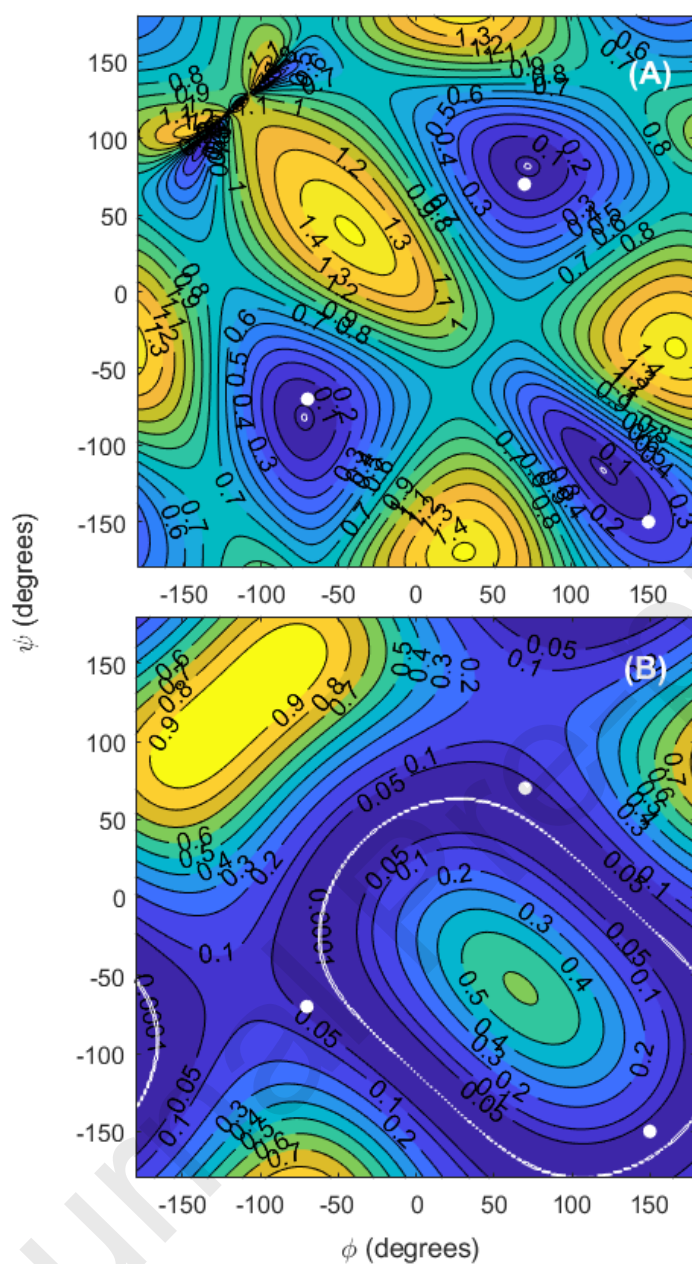
**Figure 4:** Part of WT structure showing pattern of bifurcated hydrogen bonds from the amide hydrogens of Val24-Gly25 and Lys28-Gly29 with the carbonyl oxygens of Asp23 and Asn27 on neighbouring strands, respectively.

Figure 5

	1	2	3	4	5	6	7	8	9	0	1	2	3	4	5	6	7	8	9	0	1	2	3	4	5	6	7	8	9	0	1	2	3	4	5	6	7	8	9	0
<b>WT</b>	D	A	E	F	R	H	D	S	G	Y	E	V	H	H	Q	K	L	V	F	F	A	E	D	V	G	S	N	K	G	A	I	I	G	L	M	V	G	G	V	V
<b>Dutch (E22Q)</b>	D	A	E	F	R	H	D	S	G	Y	E	V	H	H	Q	K	L	V	F	F	A	Q	D	V	G	S	N	K	G	A	I	I	G	L	M	V	G	G	V	V
<b>Iowa (D23N)</b>	D	A	E	F	R	H	D	S	G	Y	E	V	H	H	Q	K	L	V	F	F	A	N	V	G	S	N	K	G	A	I	I	G	L	M	V	G	G	V	V	
<b>Arctic (E22G)</b>	D	A	E	F	R	H	D	S	G	Y	E	V	H	H	Q	K	L	V	F	F	A	G	D	V	G	S	N	K	G	A	I	I	G	L	M	V	G	G	V	V
<b>Osaka (E22Δ)</b>	D	A	E	F	R	H	D	S	G	Y	E	V	H	H	Q	K	L	V	F	F	A	-	D	V	G	S	N	K	G	A	I	I	G	L	M	V	G	G	V	V

**Figure 5:** Alignment of WT and mutant sequences illustrating the phasing of glycines and fold directions. The grey and white columns indicate the alternating orientation of the residues along a  $\beta$ -strand. Glycines are indicated in red when on a grey residue and in blue when on a white residue. A change in the fold direction will occur at those locations where there is a change in colour of glycine. Ignoring the final glycine at position 38, for the WT, Dutch mutant and Iowa mutant there is no change in fold direction. For the Arctic mutant there are two changes of fold direction, one at Gly22 and the other at Gly25. For the Osaka mutant there is a single change in fold direction at Gly25.

Figure 6



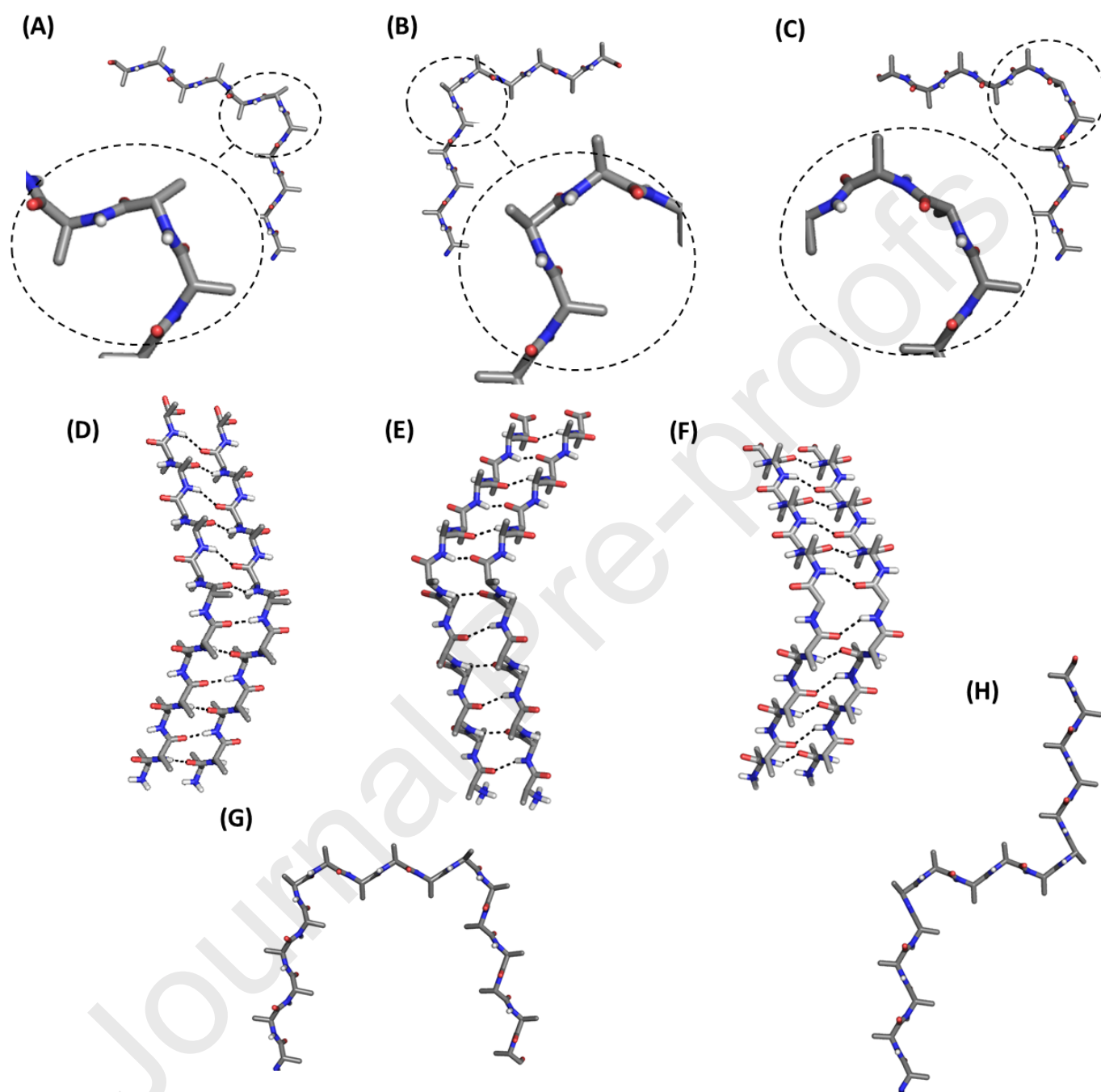
**Figure 6:** Ramachandran contour plots. The  $\phi$ ,  $\psi$  angles (sampled in  $2^\circ$  intervals) are for the residue situated at the bend between the two  $\beta$ -strands flanking the bend. The darker the colour the lower the value. The white dots are at the model values ( $-70^\circ, -70^\circ$ ),  $(70^\circ, 70^\circ)$  and  $(150^\circ, -150^\circ)$  used here for  $\alpha_R$ ,  $\alpha_L$  and  $\epsilon$ , respectively. **(A)** Contours of  $S_p$  as defined in Equation (1). Points at  $S_p = 0$  (within small white contours at  $S_p = 0.001$  in the centre of the dark blue regions) are where the peptide

planes of both  $\beta$ -strands are perpendicular to the plane defined by the two  $\beta$ -strands.

**(B)** Contours of  $S_B$  as defined in Equation (2). The  $S_B = 0$  contour in white is where the angle between the two  $\beta$ -strands is  $90^\circ$ .

Journal Pre-proofs

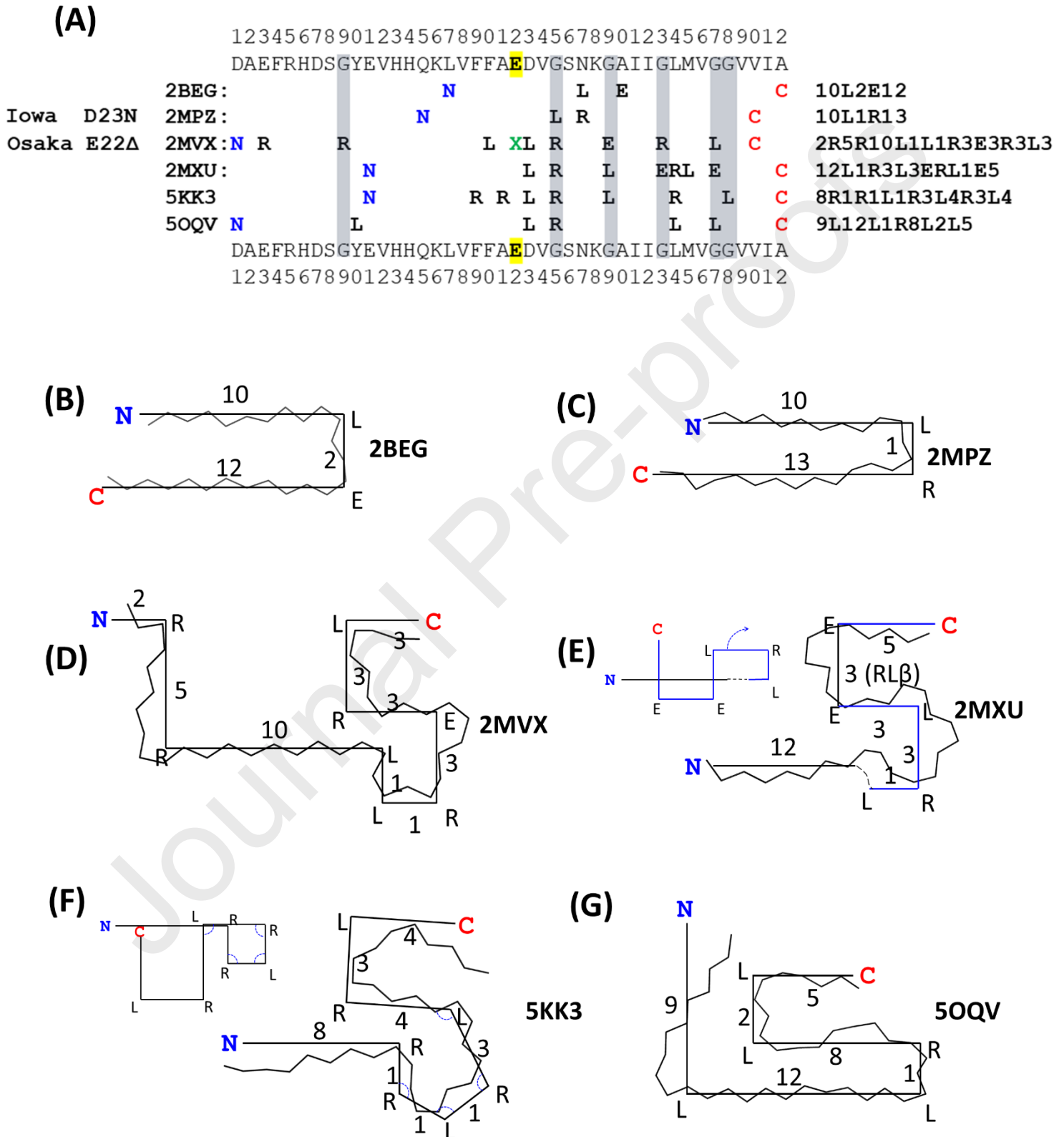
Figure 7



**Figure 7:** Half-turns in  $\beta$ -strands with  $\beta(\phi, \psi) = (-120^\circ, 115.8^\circ)$ ,  $\alpha_R(\phi, \psi) = (-70^\circ, -70^\circ)$ ,  $\alpha_L(\phi, \psi) = (70^\circ, 70^\circ)$  and  $\epsilon(\phi, \psi) = (150^\circ, -150^\circ)$ . **(A)** Left-hand half-turn:  $\cdots \beta_{\alpha_L} \beta \cdots$  **(B)** Right-hand half-turn:  $\cdots \beta_{\alpha_R} \beta \cdots$  **(C)** Left-hand half turn:  $\cdots \beta \epsilon \beta \cdots$  **(D)** Two poly-alanine strands with a  $\beta_{\alpha_R} \beta$  half-turn docked using the interactive docking tool,

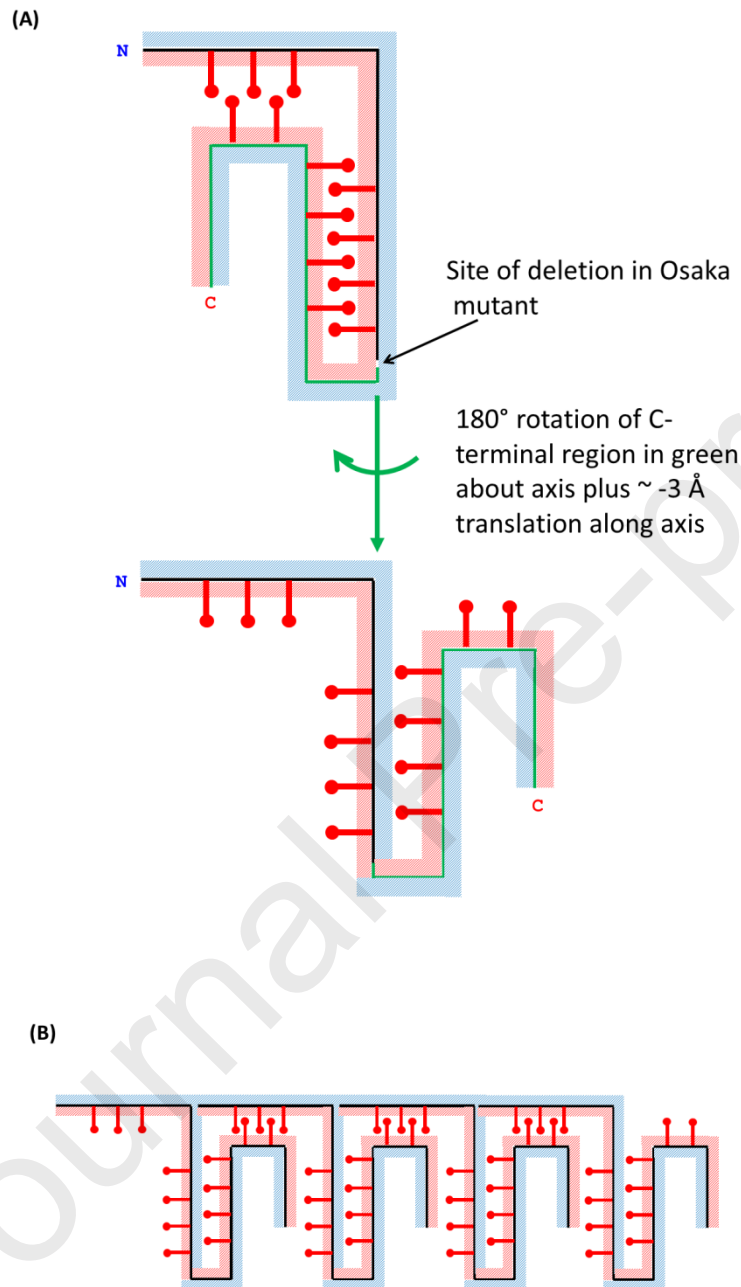
DockIT (Iakovou et al., 2020), showing all inter-strand hydrogen bonds (broken black lines), which includes those at the turn. **(E)** Similarly, for two poly-alanine strands with a  $\beta\alpha_L\beta$  half-turn. **(F)** Similarly, for two poly-alanine strands with a  $\beta\epsilon\beta$  half-turn but with the alanine at  $\epsilon$  replaced by a glycine. **(G)** Example of a “reversal”: two right-hand half-turns separated by four  $\beta$ :  $\cdots\beta\alpha_R\beta\beta\beta\alpha_R\beta\cdots$  **(H)** Example of a “crankshaft”: a right-hand half-turn and a left-hand half-turn separated by four  $\beta$ :  $\cdots\beta\alpha_R\beta\beta\beta\alpha_L\beta\cdots$

Figure 8



**Figure 8: (A)** Alignment of the half-turns in six Alzheimer A $\beta$  structures labelled by their PDB codes. “N” and “C” denote the N-terminal and C-terminal residues, respectively. A blank space between the N and C indicates the  $\beta$  or a near  $\beta$  conformation; blanks exterior to N and C represent unresolved residues. “R” indicates the right-hand half-turn,  $\beta\alpha_R\beta$ , “L”, the left-hand half-turn,  $\beta\alpha_L\beta$ , and “E”, the left-hand half-turn,  $\beta\epsilon\beta$ . The “X” in the 2MVX structure indicates the missing Glu residue in the Osaka mutant structure 2MVX. The structure of 2MPZ is the Iowa mutant and has Asn at 23 rather than Asp. The numbers in the half-turn sequences such as “10L2E12” indicate the number of residues in the  $\beta$  conformation before, between or after L, R, or E. Glycine positions are indicated with grey columns. **(B-G)** Simplified models derived from the half-turn sequences in (A) using the pairwise combination rules of Table 2 in comparison to backbone traces from the deposited PDB structures. **(B)** The 2BEG structure. **(C)** The Iowa mutant structure, 2MPZ. **(D)** The Osaka mutant structure, 2MVX. **(E)** The 2MXU structure. Inset is the half-turn sequence model which shows the structure folds in on itself. To achieve a structure close to the deposited one, the blue part rotates  $\sim 90^\circ$  about a region in the first segment that contains a run of three residues that cannot be classified as  $\beta$ ,  $\alpha_R$ ,  $\alpha_L$  or  $\epsilon$ . **(F)** The 5KK3 structure. Inset shows the half-turn sequence model which also folds in on itself. In order to achieve a structure close to the deposited one, the angles indicated in blue need to increase to  $\sim 120^\circ$ . **(G)** The 5OQV structure.

Figure 9



**Figure 9: (A)** Top: Half-turn sequence model of WT protofilament based on the 5OQV structure as seen in Figure 8(G). The half-turn sequence is 9L12L1R8L2L5. Opposite sides of the structure are indicated in red and blue and interlocking side chains (steric zipper) are indicated. The C-terminal half is indicated in green. Bottom: Half-turn sequence model of predicted Osaka mutant based on half-turn sequence, 9L11L1R8L2L5, of WT with Glu22 deleted. The green arrow indicates the screw axis about which the C-terminal half indicated in green rotates and translates in going from the WT to Osaka mutant. **(B)** Side chains from different protofilaments now interlock, joining protofilaments of the Osaka mutant model together in a domain swapping process.

Both authors devised the methods and wrote the paper. A.K. performed the Molecular Dynamics simulations and S.H. performed the structural analysis.

### Highlights

- Structural determinants of Alzheimer's A $\beta$  fibril structures are investigated.
- Three types of half-turns,  $\beta\alpha_R\beta$ ,  $\beta\alpha_L\beta$  and  $\beta\epsilon\beta$ , are shown to be main determinants
- Right-angle fold in A $\beta$  fibrils is shown to be due to cross- $\beta$  structure

- Half-turn pairwise combination rules determine backbone path and predict effect for Osaka mutant
- MD shows glycine phasing creates closed wild-type and S-shape Osaka mutant

